LMS/RVT/S26137
ESL-RPT-2019-03

Environmental Sciences Laboratory

Three Years of Multilevel Monitoring Data at the Riverton, Wyoming, Processing Site That Show Contaminant Increases After River Flooding Events and a Large Recharge Event

October 2019

U.S. DEPARTMENT OF ENERGY | Legacy Management

This page intentionally left blank

Contents

Figures

Appendixes

Abbreviations

atm	atmospheres
bgs	below ground surface
Ca	calcium
Cl	chloride
CMT	continuous multichannel tubing
CO_2	carbon dioxide
DOC	dissolved organic carbon
DOE	U.S. Department of Energy
ESL	Environmental Sciences Laboratory
ft	feet
IC	institutional control
ICP-OES	inductively coupled plasma–optical emission spectrometry
K	potassium
LM	Office of Legacy Management
Mg	magnesium
mg/L	milligrams per liter
Mn	manganese
Mo	molybdenum
Na	sodium
NRC	U.S. Nuclear Regulatory Commission
SI	saturation index
SO_4	sulfate
U	uranium
USGS	U.S. Geological Survey
VMR	Verification Monitoring Report

This page intentionally left blank

Executive Summary

The tailings pile at the Riverton, Wyoming, Processing Site has been removed, but contaminant concentrations in the shallow aquifer increase after large recharge events. The Riverton site experienced flooding near the Little Wind River in early May 2016, February 2017, and June 2017. The May 2016 flooding was from a large rain event. The February 2017 flooding was due to an ice jam, and the June 2017 flooding was due to mountain snowmelt runoff. In addition, the site experienced high water tables in April and May 2017, as this was the second wettest spring in Riverton since records began in 1918.

Past reports indicated the accumulation of solid-phase uranium and molybdenum in evaporites above the respective contaminant groundwater plumes. Given these data, multilevel monitoring wells were installed in 2015 to monitor seasonal changes in groundwater quality. Data from three years of groundwater monitoring are summarized in this report and compared with the flooding and large recharge events. The results indicate that evaporite-related constituents (especially sodium, sulfate, and chloride) present across the site in a silt layer can be released to the shallow sand and gravel aquifer during flooding and large recharge events. The solid-phase and water-phase data confirm that these evaporites are mainly sodium sulfate and sodium chloride salts with some calcite and gypsum.

All of these events likely created flow through the silt layer that enhanced the dissolution and transport of constituents in the evaporites. Depending on the amount of silt and evaporites near each respective well, these constituents either increase immediately at the top of the aquifer after an extreme event or have delayed increases in the aquifer due to nearby dissolution. A well outside the contaminant plume (0852) confirms that the formation of evaporites and the subsequent release of evaporite-related constituents to shallow groundwater is a naturally occurring process. Flooding or extreme recharge did not occur in 2018, and the groundwater quality remained relatively unchanged in that year. Thus, release of evaporite-related constituents appears to require downward flow through the typically unsaturated zone and does not occur with seasonally high water tables.

Uranium and molybdenum can be concentrated in the evaporites within the silt at the Riverton site. Naturally occurring uranium can be found in evaporites outside the uranium plume, but at lower concentrations. Thus, uranium is released to the shallow groundwater outside the plume footprint during flooding or large recharge events, but at concentrations that are much lower than those released over the uranium plume. Release of uranium outside of the uranium plume (well 0852) can exceed site standards for a period of time, depending on the interval between extreme events. Molybdenum is not found in significant concentrations in the evaporites outside of the molybdenum plume and, thus, is a more unique indicator of mill-derived contamination.

Uranium and molybdenum are released to the shallow groundwater during evaporite dissolution with flooding or large recharge events, but may have additional geochemical controls. Extended periods of high water tables (e.g., in the spring of 2017) appear to create reducing conditions at the top of the water table (top ports of multilevel wells that are typically dry) that can release manganese and iron. The data suggest that molybdenum that may have been sorbed to the manganese and iron is released to the groundwater. However, uranium concentrations are lower at the top of the water table, possibly due to stronger sorption to organic carbon with the greater reducing conditions. The change in geochemical conditions with extended high water table

conditions is also suggested by the release of dissolved organic carbon and greater carbon dioxide concentrations that can dissolve more calcite and increase the alkalinity concentrations. Overall, uranium and molybdenum release from the silt layer is likely dominated by evaporite dissolution. However, additional mechanisms, such as sorption/desorption from iron/manganese oxides and organic carbon, along with variable redox conditions, also need to be considered in evaluating contaminant transport.

Each multilevel well has subtle differences based on its location. This report summarizes the well locations in respect to the uranium and molybdenum plumes along with the differences in geochemistry seen during the three-year monitoring period. Well 0852 shows evaporite dissolution with some uranium release, but does not have molybdenum (outside of molybdenum plume). Wells 0853 and 0854 are on the edge of the uranium and molybdenum plumes. They show some potential release of uranium and molybdenum during flood or large recharge events, but trends are subtle, with molybdenum near or below the detection limit and uranium concentrations near the site standard. Wells 0855–0858 are all within the uranium and molybdenum plumes, and all show evaporite dissolution along with uranium and molybdenum release after flooding and large recharge events, with subtle differences in response timing. Because of the thick silt layer at this location, well 0855 shows a more muted concentration response with the bottom port being lower in constituent concentrations and less connected to surficial recharge events.

The implication of the multilevel well data and prior solid-phase sampling is that long-term contaminant release (with a focus on uranium and molybdenum) can be delayed by retention in the generally unsaturated silt layer. As a result, these contaminants are released only during large recharge events that force recharge water from the surface to the top of the water table. Because of uncertainty in the timing of large recharge events, prediction of the natural flushing time frame cannot be deterministic and will need to be done in a probabilistic manner. In addition to contaminant release timing, contaminant concentrations may increase in the unsaturated zone when the time between high recharge events becomes greater. Thus, contaminant release concentrations will also need to be considered in a probabilistic manner.

1.0 Introduction

A uranium and vanadium ore processing mill operated from 1958 to 1963 at the Riverton, Wyoming, Processing Site (Riverton site, Figure 1). A tailings pile covered about 72 acres of the 140-acre site (Figure 2). The tailings and associated slurry water were the primary, original source of contamination in the surficial aquifer. In 1988 and 1989, the tailings pile was excavated down to an average depth of 4 feet (ft) below ground surface (bgs) based on a radium soil standard in Title 40 *Code of Federal Regulations* Part 192 (40 CFR 192). Surface remediation activities resulted in removal of about 1.8 million cubic yards of tailings and associated materials from the site, which were encapsulated at the Gas Hills East, Wyoming, Disposal Site (Figure 1 and DOE 1998a). Soils at and below the water table with elevated thorium concentrations were left in place (DOE 1991) on portions of the former mill site as permitted by the supplemental standards provision of 40 CFR 192.

The U.S. Department of Energy (DOE) conducted initial groundwater characterization of the Riverton site in the 1990s. The characterization culminated in a Site Observational Work Plan (DOE 1998a) that recommended a natural flushing compliance strategy with an institutional control (IC) boundary (Figure 2) that limits groundwater use. The U.S. Nuclear Regulatory Commission (NRC) concurred with the natural flushing compliance strategy in the Ground Water Compliance Action Plan (DOE 1998b). DOE has conducted verification monitoring since 1998 to document site conditions and assess the progress of natural flushing. Data collected during verification monitoring are reported annually in a Verification Monitoring Report (VMR). Figure 2 shows the Riverton site features, the IC boundary, and monitoring locations from the 2018 VMR (DOE 2019).

Additional details about the Riverton site, along with links to site documents and data, can be found at https://www.lm.doe.gov/riverton/Sites.aspx. Water quality data for the Riverton site are archived in the U.S. Department of Energy Office of Legacy Management (LM) environmental database in Grand Junction, Colorado. Water quality data also are available for viewing with dynamic mapping via the Geospatial Environmental Mapping System website at https://gems.lm.doe.gov/#site=RVT.

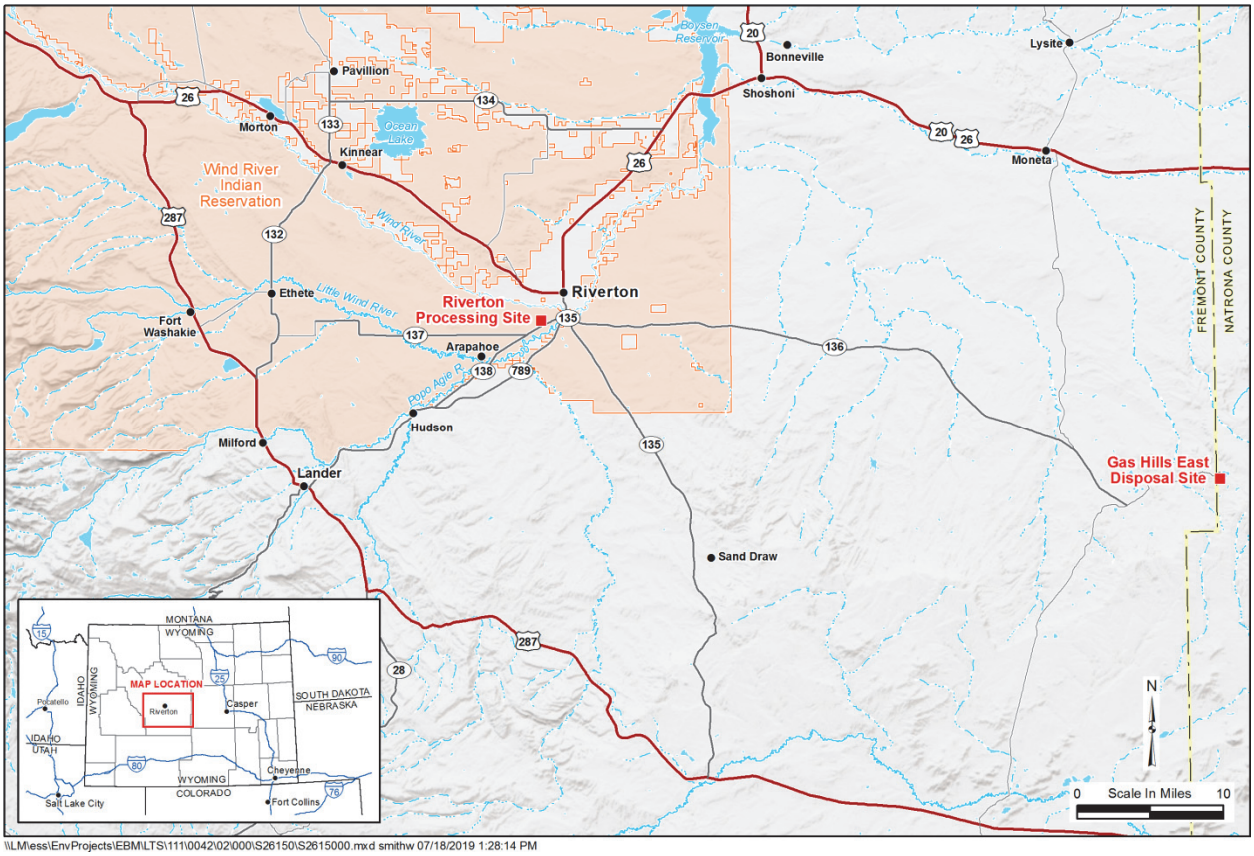

Figure 1. Riverton Site Location Map (modified from DOE 2019)

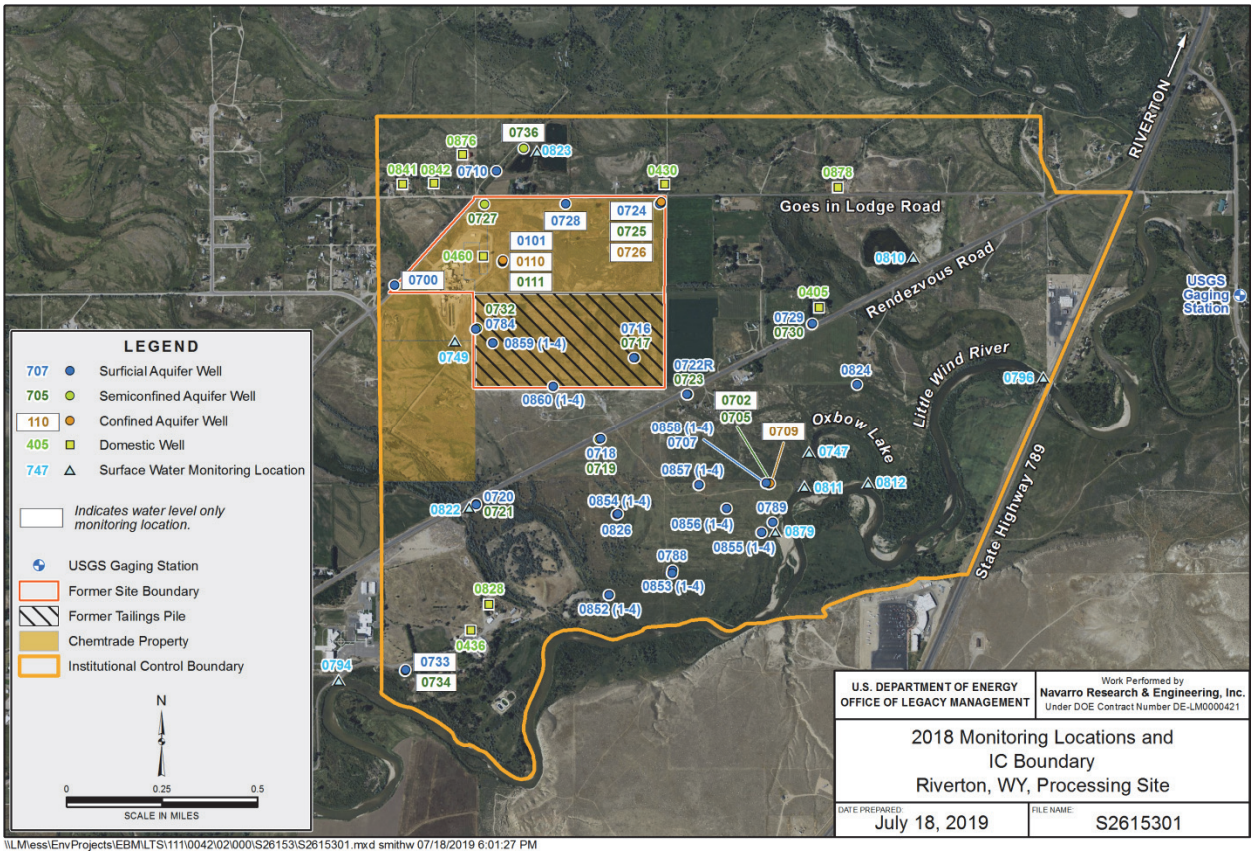

Figure 2. 2018 Monitoring Locations and IC Boundary at the Riverton Site (modified from DOE 2019)

Results of the verification monitoring indicated that natural flushing was generally progressing as expected until June 2010, when significant increases in contaminant concentrations were measured in several wells downgradient of the site after the area flooded, including well 0707 (Figure 3). In response to the unexpected results following the flood, an enhanced characterization of the surficial aquifer was conducted in 2012, which included the installation of 103 boreholes along nine transects with a direct-push drilling rig, collection of 103 water samples and 65 soil samples, laboratory tests on the soil samples, and additional groundwater modeling. Results and analysis of the enhanced characterization are reported in the *2012 Enhanced Characterization and Monitoring Report, Riverton, Wyoming, Processing Site* (DOE 2013). Additional work was completed in 2015 and is summarized in the *2015 Advanced Site Investigation and Monitoring Report, Riverton, Wyoming, Processing Site* (DOE 2016). The advanced site investigation report summarizes additional investigation in 2015 through the use of backhoe trenching, sonic drilling, multilevel monitoring wells, direct-push drilling, and temporary well points to collect soil and groundwater samples. An additional report, *Evaluation of Mineral Deposits Along the Little Wind River, Riverton, Wyoming, Processing Site* (DOE 2014) measured uranium and molybdenum concentrations in surficial evaporites.

Results from DOE 2013 and DOE 2016 indicated the presence of evaporites in a silt layer. This silt layer is generally at or near the top of the water table in the surficial aquifer, which allows for wicking of groundwater into the silt layer followed by evapotranspiration in this semiarid environment. This process naturally forms evaporites in the area, and tends to concentrate uranium and molybdenum in the silt layer over the contaminant plume, which can subsequently

be released during flooding events (DOE 2016). Likewise, surficial evaporites have higher uranium and molybdenum concentration over their respective groundwater plumes. The Riverton site conceptual model has been reevaluated to include these persistent secondary contaminant sources as a contributor to ongoing groundwater contamination that delay natural flushing (Dam et al. 2015).

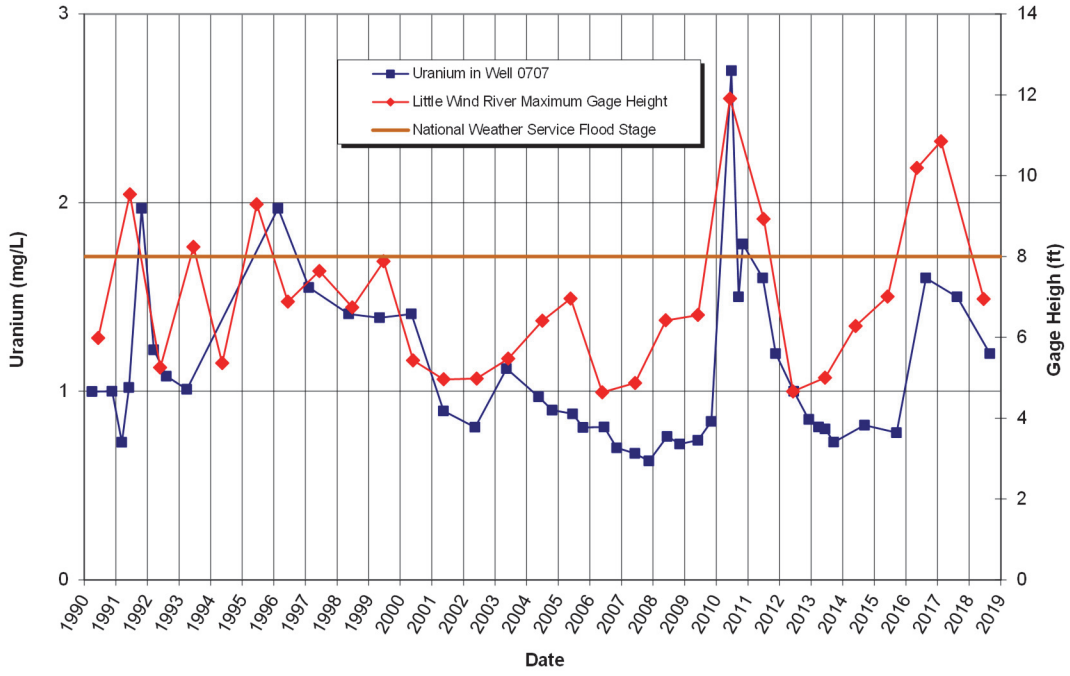

Figure 3. Uranium Concentrations in Monitoring Well 0707 Versus Little Wind River Stage

In order to evaluate the influence of seasonal variations, including flooding events, on groundwater quality with depth, discrete zone multilevel groundwater monitoring wells were installed in nine of the sonic boreholes (0852–0860, Figure 2). A "-1" indicates the shallowest sampling port, and a "-4" indicates the deepest sampling port. Multilevel monitoring wells 0852–0858 have subsequently been sampled for 3 years, with wells 0855–0858 (directly in the contaminant plume) being sampled on close to a monthly basis, with less frequent sampling for wells 0852–0854. Well 0852 is outside the uranium and molybdenum contaminant plume, and wells 0853 and 0854 are just within the edge of the contaminant plume (DOE 2016). Multilevel monitoring wells 0859 and 0860 were completed within the footprint of the former tailings impoundment, but are not influenced by flooding and are not discussed in this report. These wells are sampled on an annual basis, with sample data being reported in annual VMRs (e.g., DOE 2019).

Uranium and molybdenum are considered the key contaminants of concern at the Riverton site. The latest uranium and molybdenum plume maps from 2018 (DOE 2019) are provided for reference (Figure 4 and Figure 5). In Figure 4, well 0852 is above the groundwater uranium standard of 0.044 milligrams per liter (mg/L), but the uranium at this location is naturally occurring (DOE 2016). These figures plot the highest measured concentrations from the multilevel wells or with nearby, colocated standard monitoring wells (DOE 2019). For colocated wells (0788 and 0853; 0707 and 0858), only the highest contaminant concentrations were used in

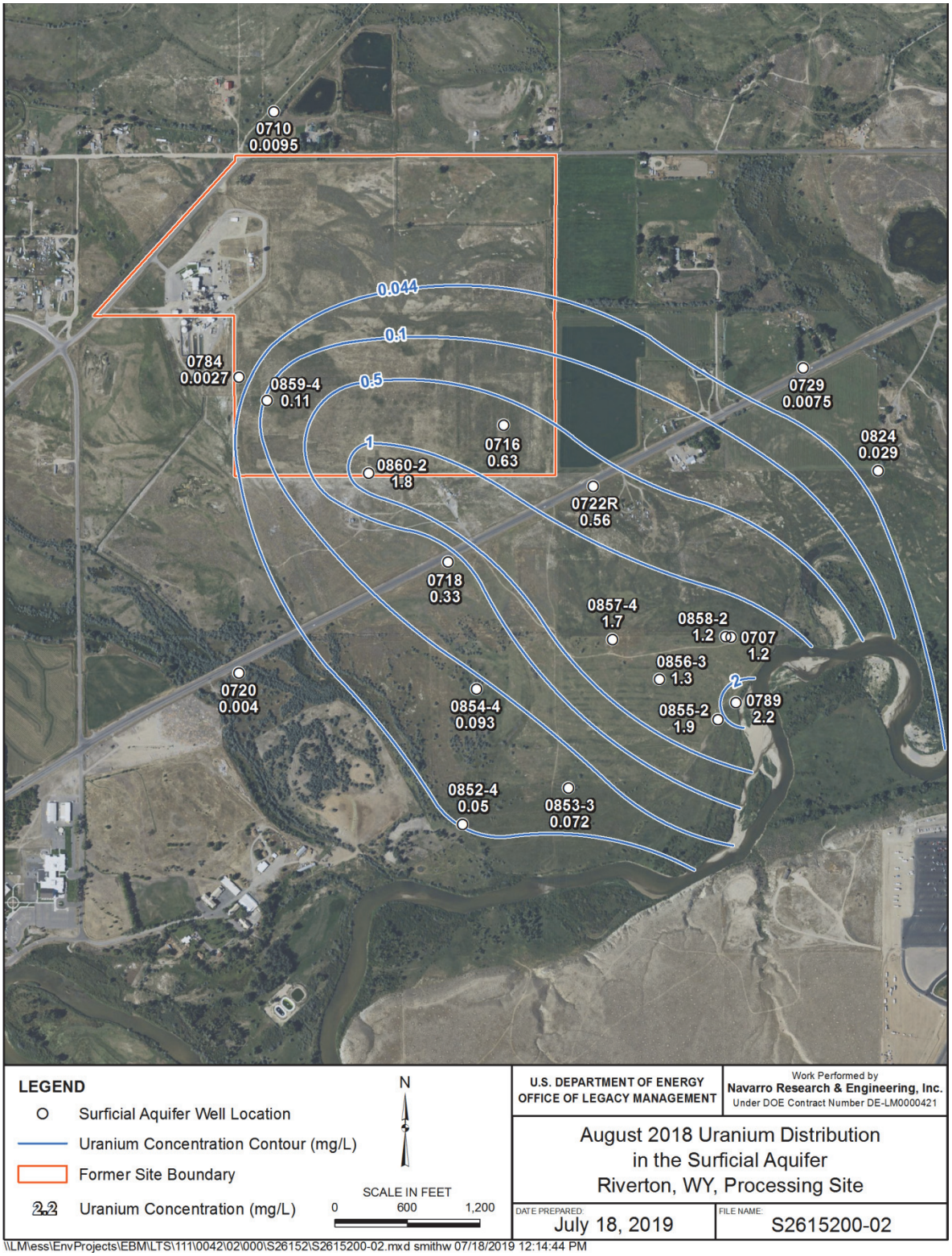

Figure 4. Uranium Distribution in the Surficial Aquifer at the Riverton Site in August 2018 (after DOE 2019)

Figure 5. Molybdenum Distribution in the Surficial Aquifer at the Riverton Site in August 2018 (after DOE 2019)

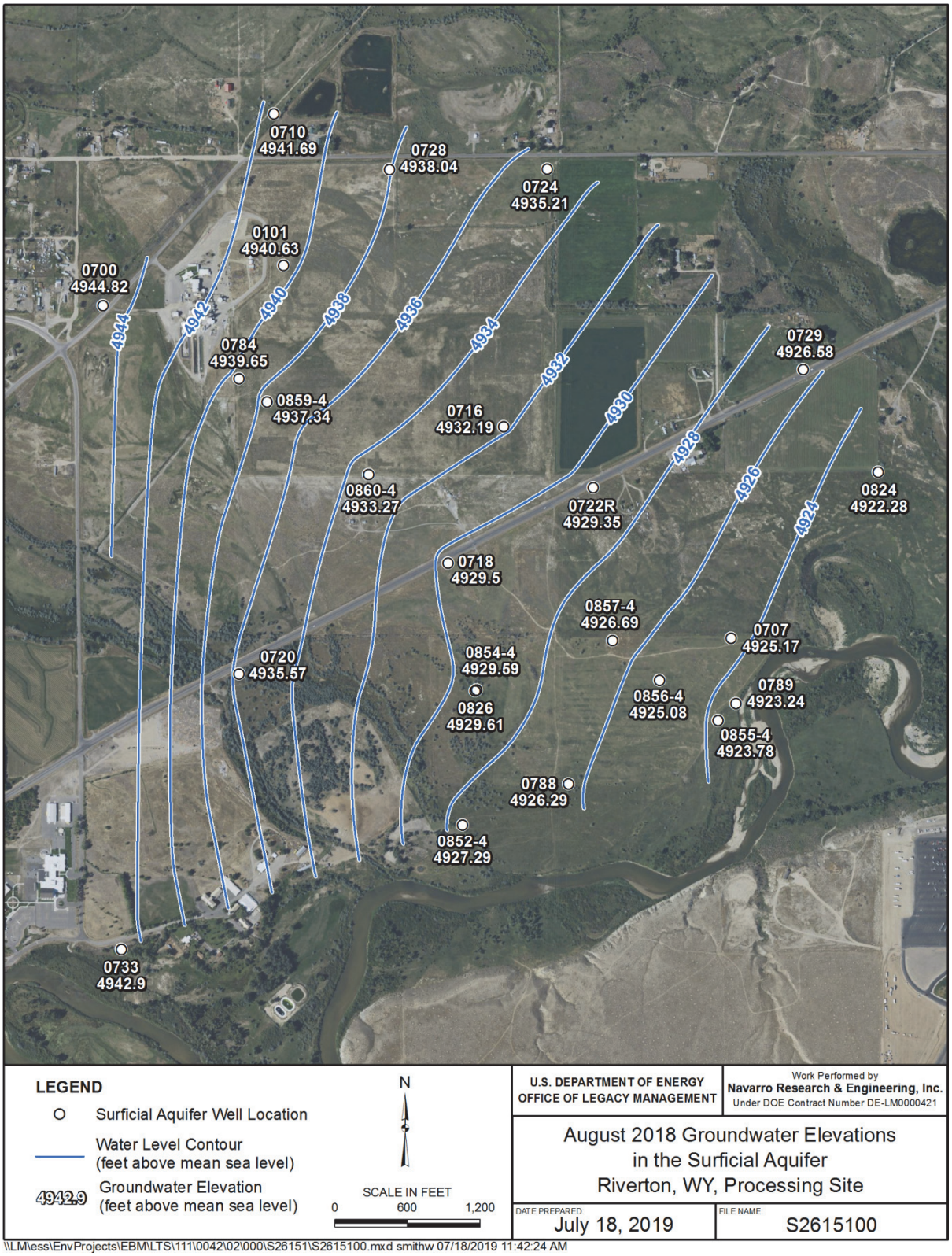

Figure 6. August 2018 Groundwater Elevations in the Surficial Aquifer at the Riverton Site (DOE 2019)

the original contouring (DOE 2019), but the multilevel well data are also posted specifically for this report (Figure 4 and Figure 5). The groundwater elevations from August 2018 (DOE 2019) are shown in Figure 6, which indicate groundwater flow in the surficial aquifer towards the southeast, with discharge to the Little Wind River.

This report summarizes the geochemical results and interpretations in wells 0852–0858 from September 15, 2015, through September 11, 2018. These geochemical results are compared with groundwater elevation changes that occurred due to flooding events caused by runoff from mountain snowmelt, large precipitation events, and a river ice jam. Overall, the largest geochemical changes occurred with the highest groundwater elevations related to flooding events in 2016 and 2017. Flooding did not occur in 2018, and groundwater geochemical changes were minimal in that year.

2.0 Methods

2.1 Multilevel Well Installation

Each well was constructed by combining a 1.5-inch well made of PVC plastic pipe with a three-channel continuous multichannel tubing (CMT) well to make a four-port multilevel monitoring well. The CMT material was secured to a 1.5-inch schedule 40 PVC pipe to allow vertical installation of the CMT material and to provide an additional monitoring port. The four sampling zones were (1) in the area of the aquifer that is only saturated during high water (typically less than 4 ft bgs), (2) near the top of the saturated zone during low groundwater elevations, (3) at the approximate midpoint of the typical saturated thickness, and (4) at the base of the surficial aquifer (with the 1.5-inch PVC and a 1 ft screened interval). CMT screen intervals were 0.5 ft and were custom cut in the field based on the lithology determined by the onsite geologist. All multilevel monitoring wells were developed by alternately surging and pumping after installation, with the following exceptions: the top ports of all multilevel monitoring wells were not developed because the ports were dry (by design) at the time of installation. All multilevel well completion details are provided in DOE 2016.

2.2 Sampling Procedures

Sampling of the multilevel wells was completed using low-flow sampling, with flow rates near 10–50 milliliters (mL) per minute to provide minimal drawdown in water levels within each port. Field parameters (pH, temperature, oxidation–reduction potential, dissolved oxygen) were measured using a multiparameter probe in a flow-through cell to reduce atmospheric contact. Alkalinity was measured immediately in the field. Groundwater samples were field filtered to less than 0.45 microns and collected in two 125 mL plastic (HDPE) bottles, one acidified with nitric acid to a pH <2 for cation and metals analyses, and one unacidified for anion analyses. All field sampling was performed by U.S. Geological Survey (USGS) personnel from the local Riverton, Wyoming, office, and samples were sent to the LM Environmental Sciences Laboratory in Grand Junction, Colorado. Multilevel well sampling occurred from September 15, 2015, to September 11, 2018.

2.3 Analytical Procedures

Groundwater samples were analyzed for site contaminants of concern (manganese [Mn], molybdenum [Mo], sulfate [SO_4], and uranium [U]), major cations (calcium [Ca], magnesium [Mg], potassium [K], and sodium [Na]), an additional major anion (chloride [Cl]), dissolved organic carbon (DOC), and field measurements of temperature, pH, specific conductance, oxidation–reduction potential, dissolved oxygen, and alkalinity at each sampling location. Laboratory analyses were completed at the LM Environmental Sciences Laboratory (ESL) in Grand Junction, Colorado, following the procedures listed below and as documented in the *Environmental Sciences Laboratory Procedures Manual* (LMS/PRO/S04343). Cations and metals were analyzed by inductively coupled plasma–optical emission spectrometry (ICP-OES) using a Perkin Elmer 7000 DV instrument (ESL Procedure AP(ICP-1)). Anions were analyzed via ion chromatography using a Dionex Aquion ion chromatograph (ESL Procedure AP(IC-3)), and dissolved organic carbon was analyzed by combustion-oxidation following acid pretreatment to remove inorganic carbon using a Shimadzu TOC-L instrument (ESL Procedure AP(NPOC-1). Uranium was analyzed by kinetic phosphorescence using a Chemchek KPA-11 instrument (ESL Procedure (AP(U-2)). September 2015 samples were sent to a DOE Consolidated Audit Program (DOECAP)–certified laboratory that used ICP-OES (EPA method 6010), inductively coupled plasma–mass spectrometry (EPA method 6020), and ion chromatography (EPA method 9056). All of the data presented in this report were analyses from the ESL, except those for September 2015, which were contract lab analyses that followed the same general procedures as listed above. However, the contract lab used an inductively coupled plasma mass spectrometer for cations and metals analyses that resulted in lower detection limits, which is especially apparent for molybdenum.

2.4 Geochemical Modeling

The geochemical modeling code PHREEQC (Parkhurst and Appelo 2013) was used for initial geochemical evaluations of potential mineral dissolution or precipitation, along with calculating carbon dioxide (CO_2) concentrations. These evaluations used the geochemical database minteqa4.dat included with the PHREEQC version 3 program download.

River Stage, Precipitation, and Groundwater Elevations Data

River stage was retrieved from the U.S. Geological Survey website (https://waterdata.usgs.gov/usa/nwis/uv?site_no=06235500) for site USGS 06235500 LITTLE WIND RIVER NEAR RIVERTON, WY (hence referred to as the Little Wind River gage and shown in Figure 2) and USGS 06228000 WIND RIVER AT RIVERTON, WY (https://waterdata.usgs.gov/nwis/uv?site_no=06228000 (hence referred to as the Wind River gage). Precipitation data was retrieved for the National Oceanic and Atmospheric Administration weather station in Riverton, Wyoming, station GHCND: USC00487760 (https://www.ncdc.noaa.gov/cdo-web/datasets/GHCND/stations/GHCND:USC00487760/detail). Groundwater elevations were measured in the 1.5-inch PVC center stock for each multilevel well before sampling. Wells 0707, 0855-4, 0856-4, and 0857-4 had continuous groundwater elevation data loggers.

3.0 Results and Discussion

3.1 River Stage, Precipitation, and Groundwater Elevations

The main controls on the Little Wind River stage (and discharge) are runoff from precipitation events, runoff from mountain snowmelt, and ice jams. River base flow (lower stage) is controlled by groundwater discharge within the river basin. Groundwater elevation at the Riverton site is controlled mainly by the stream water elevation of the nearby Wind River and Little Wind River (DOE 1998a). The Little Wind River is closer to the Riverton site than the Wind River and has an annual spring peak in gage height (and discharge) that is controlled by snowmelt runoff from the nearby Wind River Mountain range. Flood stage for the Little Wind River gage is 8 feet. During the period of multilevel well sampling, the Little Wind River gage had peak flooding conditions on May 8, 2016, February 10, 2017, and June 9, 2017 with gage heights of 10.19, 10.86, and 9.81 ft, respectively. The peak height for the Little Wind River gage in 2018 was 6.95 ft on June 19, 2018. These event dates are highlighted and labeled in Figure 7. These same dates are highlighted in subsequent figures as a reference, but without repeating the direct date labels. Before May 8, 2016, flooding on the Little Wind River had not occurred since July 2, 2011, with a stage of 11.80 ft (Figure 3).

Several other Little Wind River gage heights are notable, but not separately labeled in Figure 7. After the early spring flood event on May 8, 2016, the Little Wind River exceeded flood stage slightly at 8.21 ft on June 11, 2016, because of snowmelt runoff. In 2017, after the June 9, 2017, snowmelt runoff peak of 9.81 ft, a second snowmelt-related flood stage peak of 9.71 ft occurred on June 19, 2017. In 2018, the initial snowmelt runoff peak was a gage height of 6.91 ft on June 1, 2018, compared to the gage height of 6.95 ft on June 19, 2018 (labeled in Figure 7).

Riverton, Wyoming, precipitation data is added to the Little Wind River stage in Figure 8 to evaluate precipitation events. The May 8, 2016, stage peak was before the mountain snowmelt peak (June 11, 2016) and was triggered by a significant rain event with 1.45 inches of rain reported in Riverton on May 7, 2016. Local precipitation was also relatively high starting on March 29, 2016 (Figure 8), with a snow event on March 29 and 30, 2016, with 0.61 and 1.06 inches of liquid-equivalent precipitation. This snow quickly melted, with no snow on the ground at the Riverton weather station by April 3, 2016. Additional rain/snow events with snow cover of only 1 inch occurred on April 19 and 20, 2016 (0.59 inches of liquid equivalent), and April 24–27, 2016 (2.78 inches of liquid equivalent), plus a rain event of 0.51 inches on April 30 and May 1, 2016. All of these events created a limited change in the Little Wind River stage (Figure 8), whereas the rain event starting on May 7, 2016, did create sudden flooding conditions, presumably due to significant runoff from saturated ground conditions. In addition, upstream rainfall was even more significant with Lander, Wyoming, receiving 0.69 inches of rain on May 6, 2017, 3.35 inches of rain May 7, 2016, and 0.41 inches of rain on May 8, 2016, which contributed to the flooding conditions on May 8, 2016, on the Little Wind River. For reference, the average total precipitation for Riverton, Wyoming, is 8.42 inches, and the spring of 2016 ranked as the wettest spring (March, April, May) on record from 1918 to 2016 with 9.11 inches of precipitation and the second wettest year on record at 15.24 inches of precipitation (https://www.weather.gov/riw/Riverton2016ClimateSummary).

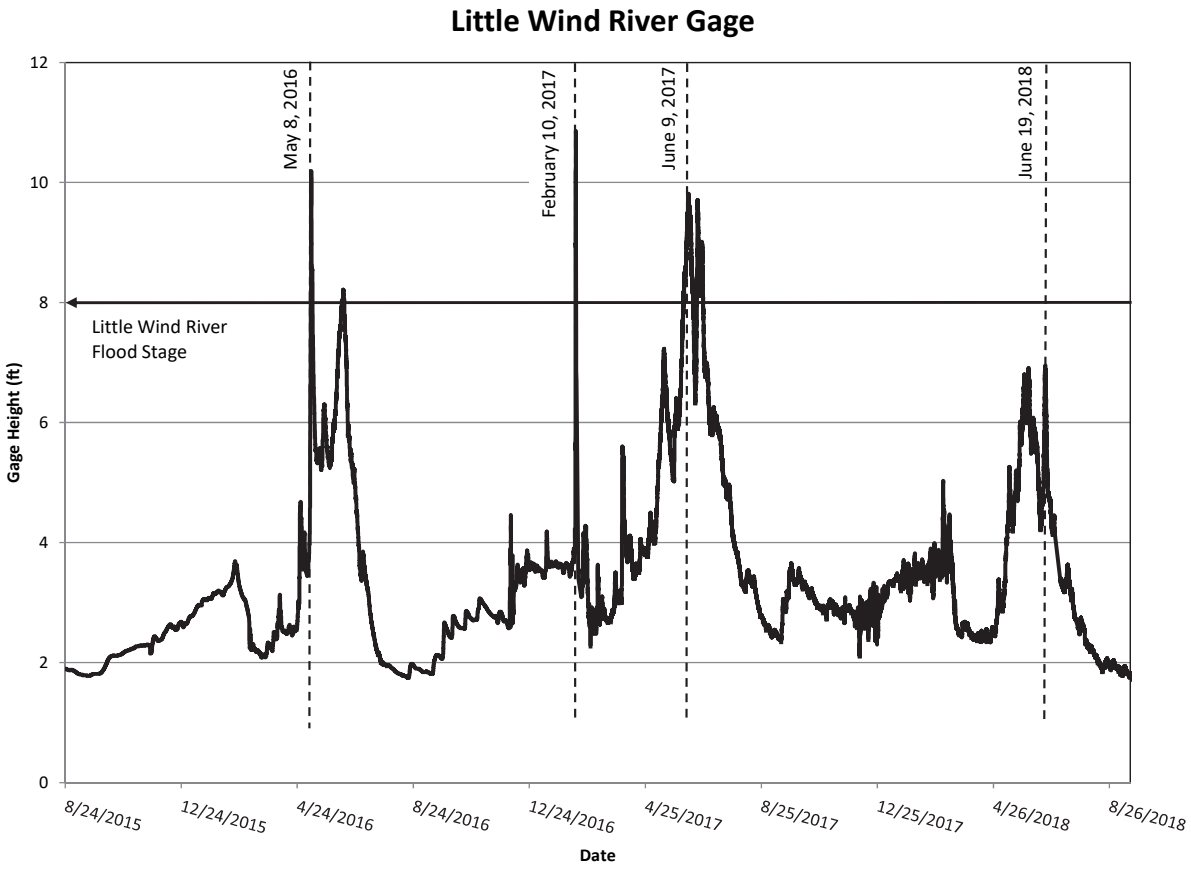

Figure 7. Gage Heights for the Little Wind River

On the Little Wind River in 2017, the first flooding event occurred on February 10, 2017, due to an ice jam. This flooding was very brief in duration (Figure 8). In Riverton, Wyoming, 2017 was also a very wet spring and became the second wettest spring (March, April, May) on record from 1918 to 2017, after 2016, with 8.49 inches of precipitation. The year 2017 became the new second wettest year on record since 1918 at 15.86 inches of precipitation.[1] The most significant spring rain event was 1.5 inches of rain on March 31, 2017, followed by 1.37 inches of rain on April 1, 2017. This event created a brief increase in the Little Wind River stage (Figure 8). Spring precipitation was then followed by flooding due to runoff of mountain snowmelt with peak gage heights on June 9 and 19, 2017, as previously discussed.

In 2018, Riverton, Wyoming, had a wet May, with 3.63 inches of precipitation compared to a normal of 1.45 inches. May is typically the wettest month of the year in Riverton. Overall precipitation for the year was 8.94 inches, which is close to average.[2] The wet May in 2018 likely contributed to a slightly earlier rise in the Little Wind River stage, but combined with modest runoff from mountain snowmelt did not produce flood conditions (Figure 8).

[1] https://www.weather.gov/riw/Riverton2017ClimateSummary.
[2] https://www.weather.gov/riw/Riverton2018ClimateSummary.

The above discussion on hydrology of the Little Wind River and precipitation data for Riverton, Wyoming, in 2016 through 2018 is provided as a basis for interpreting the groundwater elevation data and whether or not flow through the typically unsaturated zone is a possibility. In summary, key events are (1) flooding on May 8, 2016, from a wet spring and a large rain event in the Little Wind River basin at lower elevations, (2) flooding on February 10, 2017, from an ice jam, (3) very wet spring in 2017, (4) flooding on June 9, 2017, with a second flood peak on June 19, 2017, from runoff from mountain snowmelt, and (5) a more typical river stage and precipitation in 2018 (Figure 7 and Figure 8). These events are reflected in the groundwater elevation in well 0707 (Figure 9), indicating strong control of shallow groundwater elevations by the stage of the Little Wind River at this well. Well 0707 is 380 feet from the bank of the Little Wind River.

The March 31 and April 1, 2017, rain events along with a wet spring overall are large precipitation events with a measurable, but relatively limited river response (Figure 8); thus, this is a large recharge event to shallow groundwater. This event is apparent with a sudden increase in groundwater elevation at well 0707 on March 31, 2017 (Figure 9), with groundwater elevations that are maintained at a higher elevation without Little Wind River stage control (Figure 10). This high groundwater elevation in the spring of 2017 was captured in data loggers across the site, including in wells away from the Little Wind River and upgradient from well 0707 (data for wells 0710, 0101, and 0722R are provided in Appendix A). The hydrograph for well 0101, which is about 5200 feet from the Little Wind River, is also provided in Figure 11. This well shows a much more muted response to the stage of the Little Wind River, but does show a strong response to the large recharge in the spring of 2017 (Figure 11). In addition, a comparison of the Little Wind River and Wind River gage heights (Figure 12) confirms that the April 2017 increases in groundwater elevations across the site are not controlled by the Wind River. In fact, the Wind River does not appear to have any control on groundwater elevation on well 0101 (Figure 11 and Figure 12, especially note the time periods of April 1 to June 1, 2017 [well response due to recharge which is not seen in the Wind River stage], and December 21, 2017 to March 17, 2018 [change in Wind River stage that is not seen in well 0101 groundwater elevations]).

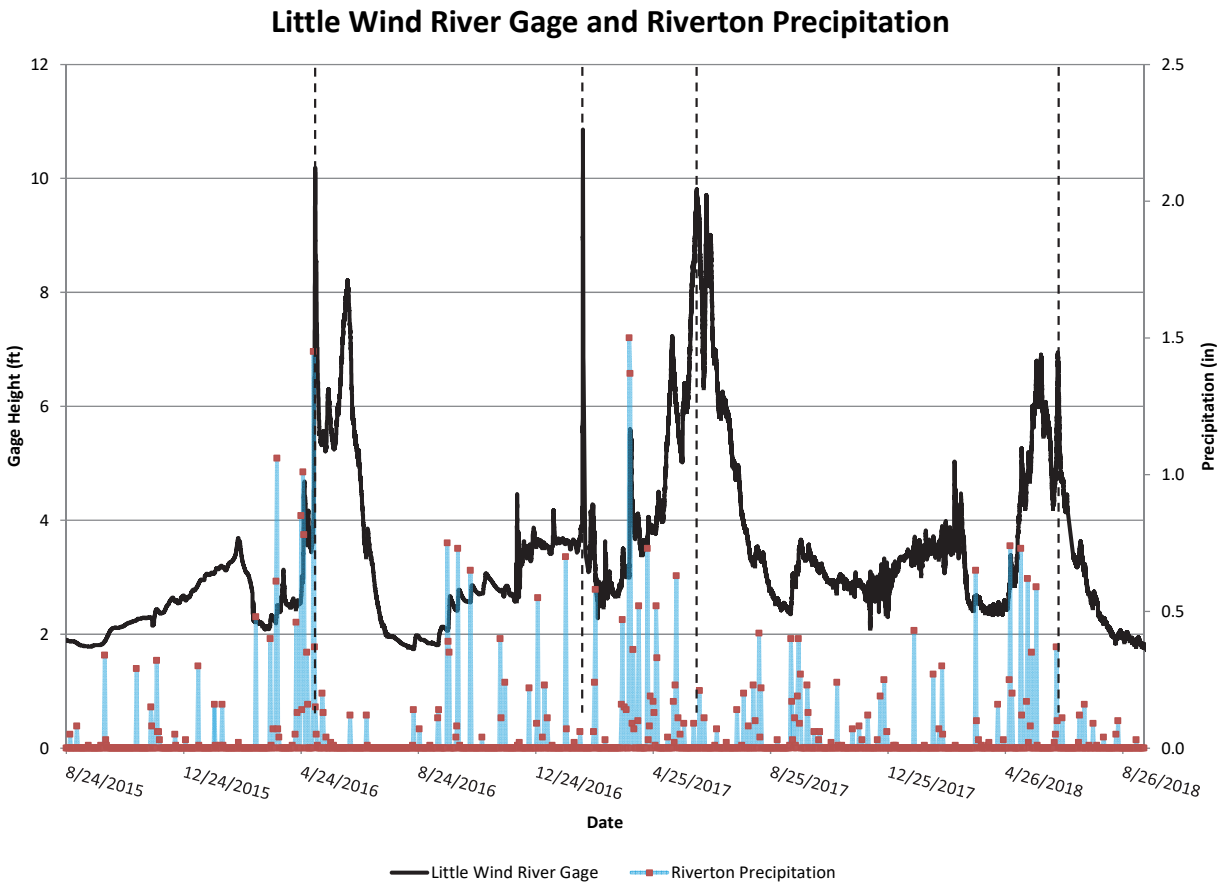

Figure 8. Gage Heights for the Little Wind River Along with Precipitation in Riverton, Wyoming

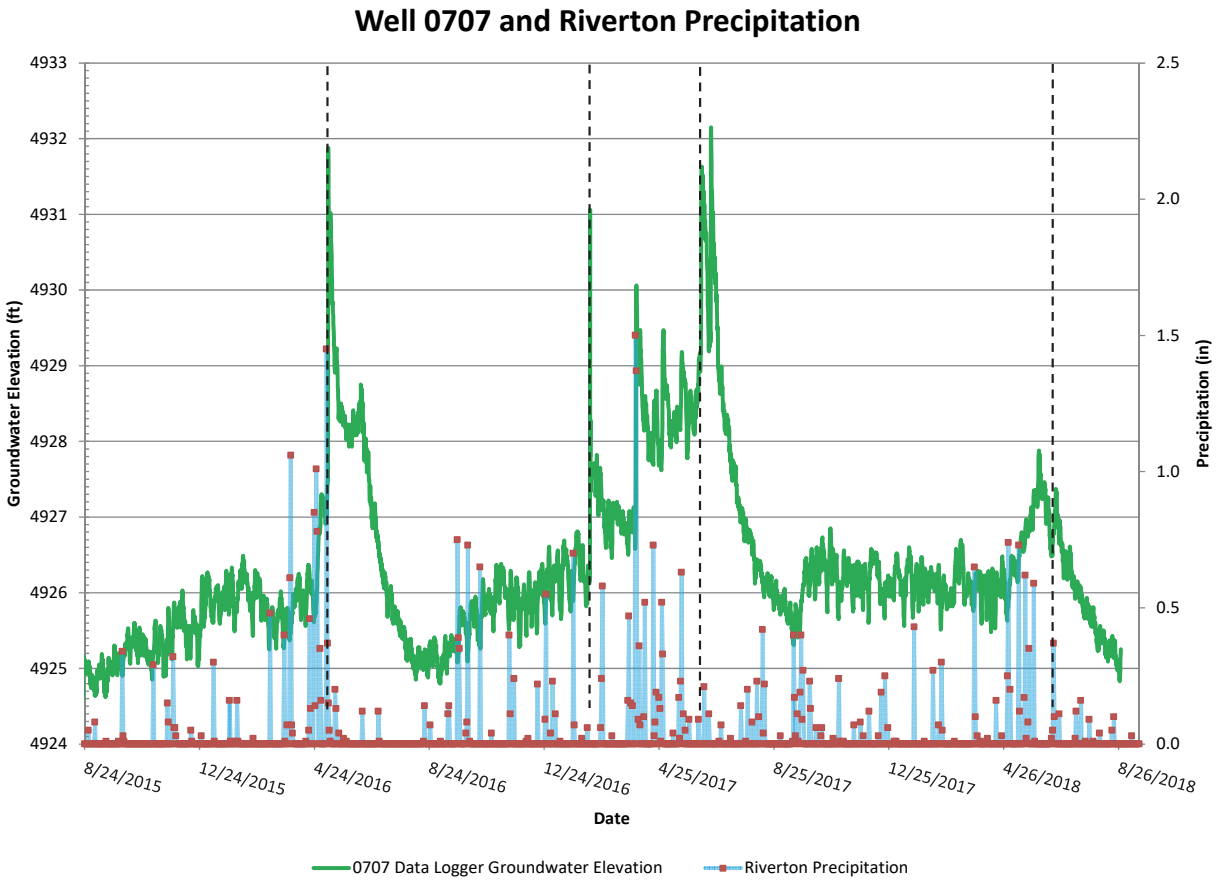

Figure 9. Well 0707 Hydrograph with Precipitation in Riverton, Wyoming

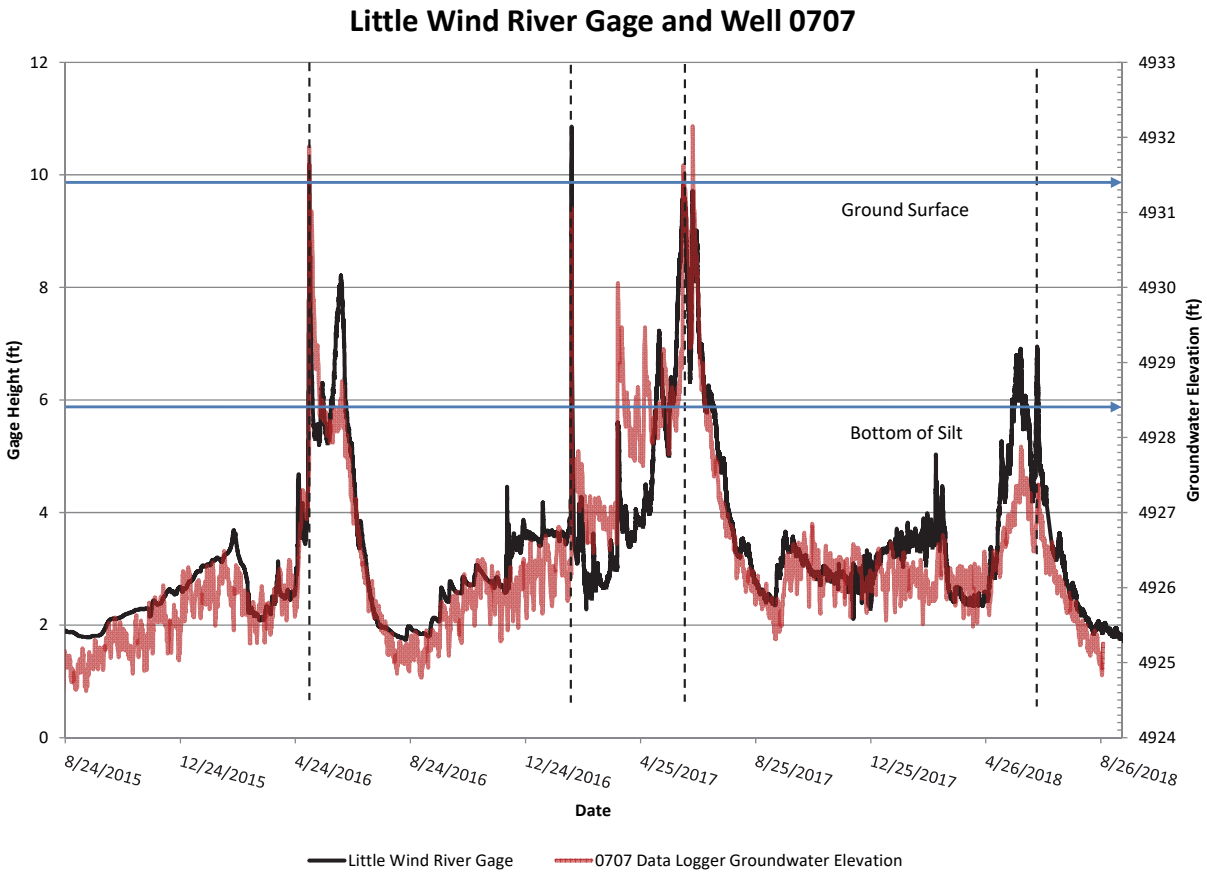

Figure 10. Well 0707 Hydrograph with Little Wind River Gage Heights

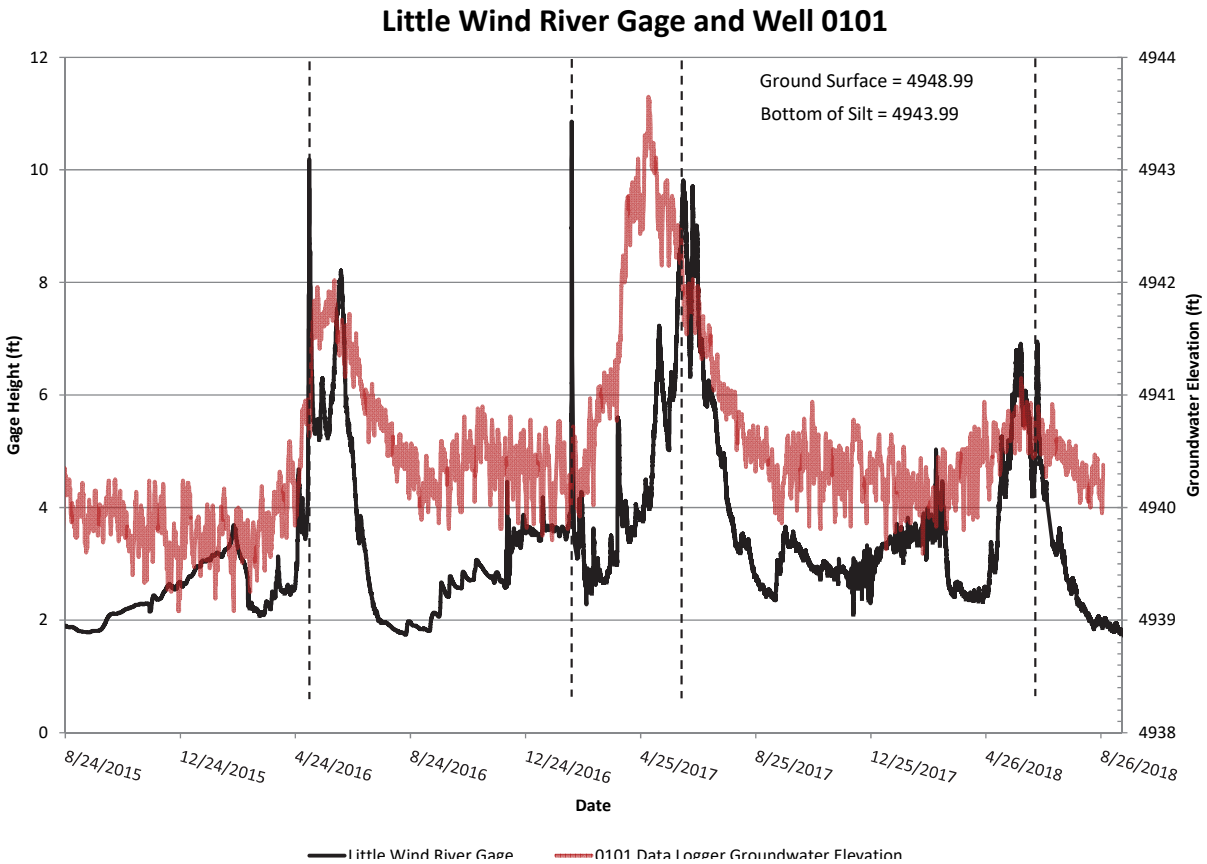

Figure 11. Well 0101 Hydrograph with Little Wind River Gage Heights

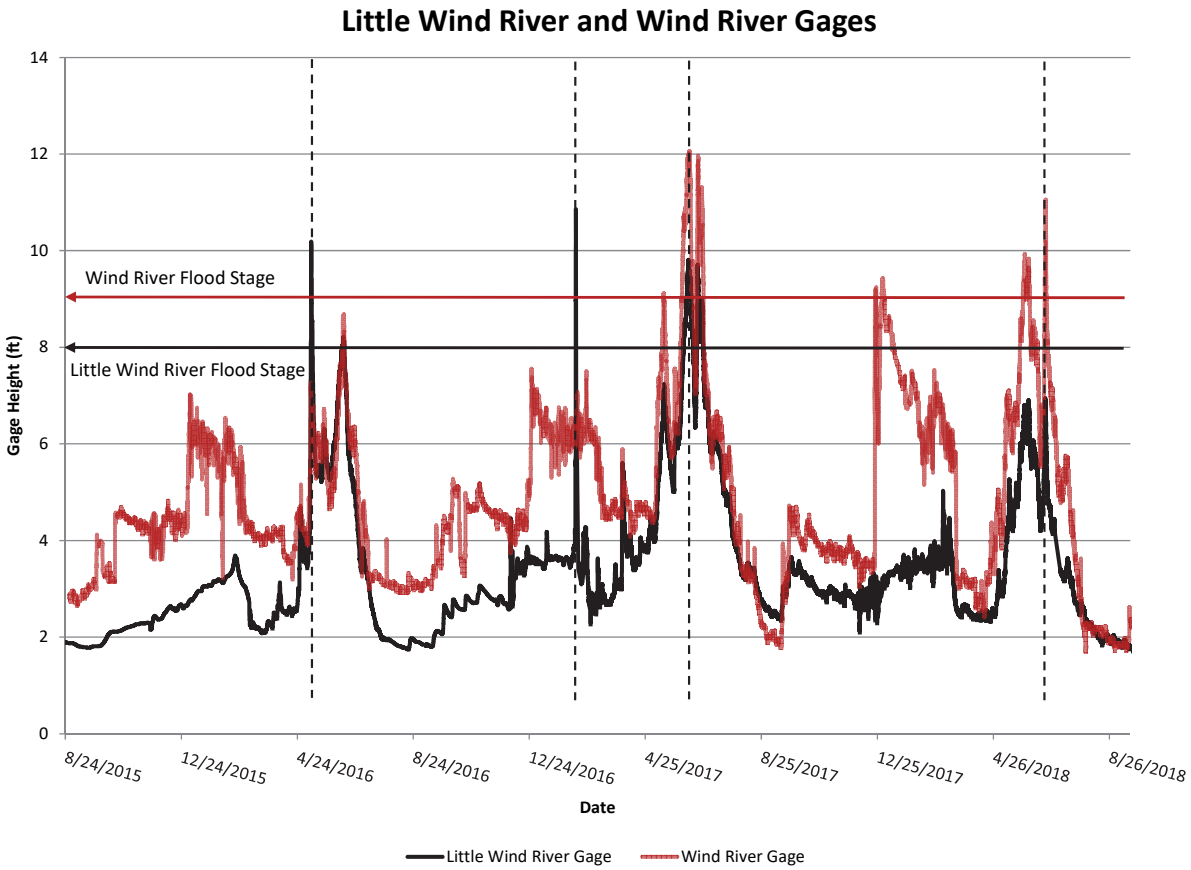

Figure 12. Little Wind River and Wind River Gage Heights

3.2 Hydrology in Multilevel Wells

Hydrographs for wells 0852–0858 compared with the stage in the Little Wind River are provided in Appendix B. These figures provide all available data on groundwater elevations from data loggers and manual water-level measurements. Since a silt layer across the site has the potential to store contaminants (DOE 2016, and Dam et al. 2015), all the hydrographs in Appendix B have the bottom of the silt layer noted based on drilling logs (DOE 2016) along with the ground surface. Elevations of the ground surface and the bottom of the silt layer are also noted for wells 0707 and 0101 in Figure 10 and Figure 11, respectively. For well 0857, no silt was indicated in the well log; thus, the layer indicated as silty gravel has been noted.

Wells 0852, 0853, and 0854 are on the edge of the uranium plume (Figure 4), so they did not have data loggers installed and were not sampled as frequently as wells 0855–0858. Detailed groundwater elevation trends in wells 0852, 0853, and 0854 are difficult to determine, but the hydrographs generally follow river stage. Flooding at wells 0852 and 0853 in 2016 and 2017 was visually confirmed, and well 0854 was at the edge of the flooding based on verbal report from USGS personnel. On all three wells it is apparent that groundwater did contact the bottom of the silt layer in 2016 and 2017. Groundwater contact with the silt layer in 2018 could have occurred briefly, in these three wells, but was not measured directly (Appendix B).

Data loggers were installed in wells 0855, 0856, and 0857 in August of 2016. Well 0858 is essentially colocated with well 0707 (see hydrograph in Figure 10). Wells 0855, 0856, and 0858 had flood waters at the ground surface in 2016 based on visual confirmation by USGS personnel, which was then confirmed again in 2017 with hydrograph data and visual confirmation. Well 0857 was at the edge of the flood waters in 2016 and 2017 (visual and hydrograph data). Wells 0855–0858 are all strongly controlled by the river stage. Well 0855 is the closest to the Little Wind River and is most strongly controlled by river stage (Figure 13), whereas well 0857 is the farthest from the Little Wind River and shows a slightly more muted response to river stage (Figure 14). Wells 0856 (Appendix B), 0857 (Figure 14), and 0858 (Appendix B and colocated well 0707 in Figure 11) all show the high groundwater elevations from March 31 through May 31, 2017, due to recharge from spring precipitation that was discussed earlier.

Well 0855 has a thick silt layer, and groundwater elevation is always above the bottom of the silt (Figure 13). Well 0857 only has a silty gravel zone with the groundwater elevation close to or above the bottom of that layer during 2016 flooding, above the bottom of that layer during the high spring groundwater elevations in 2017, and below the bottom of the layer in 2018 (Figure 14). Wells 0856 and 0858 clearly had groundwater above the bottom of the silt layer due to flooding conditions in 2016 and 2017. The seasonally high groundwater elevation in the spring of 2018 was about 1 ft below the bottom of the silt layer in 0856 (Appendix B) and about 0.3 ft below the bottom of the silt layer in 0858 (based on highest groundwater elevation in well 0707, Figure 11).

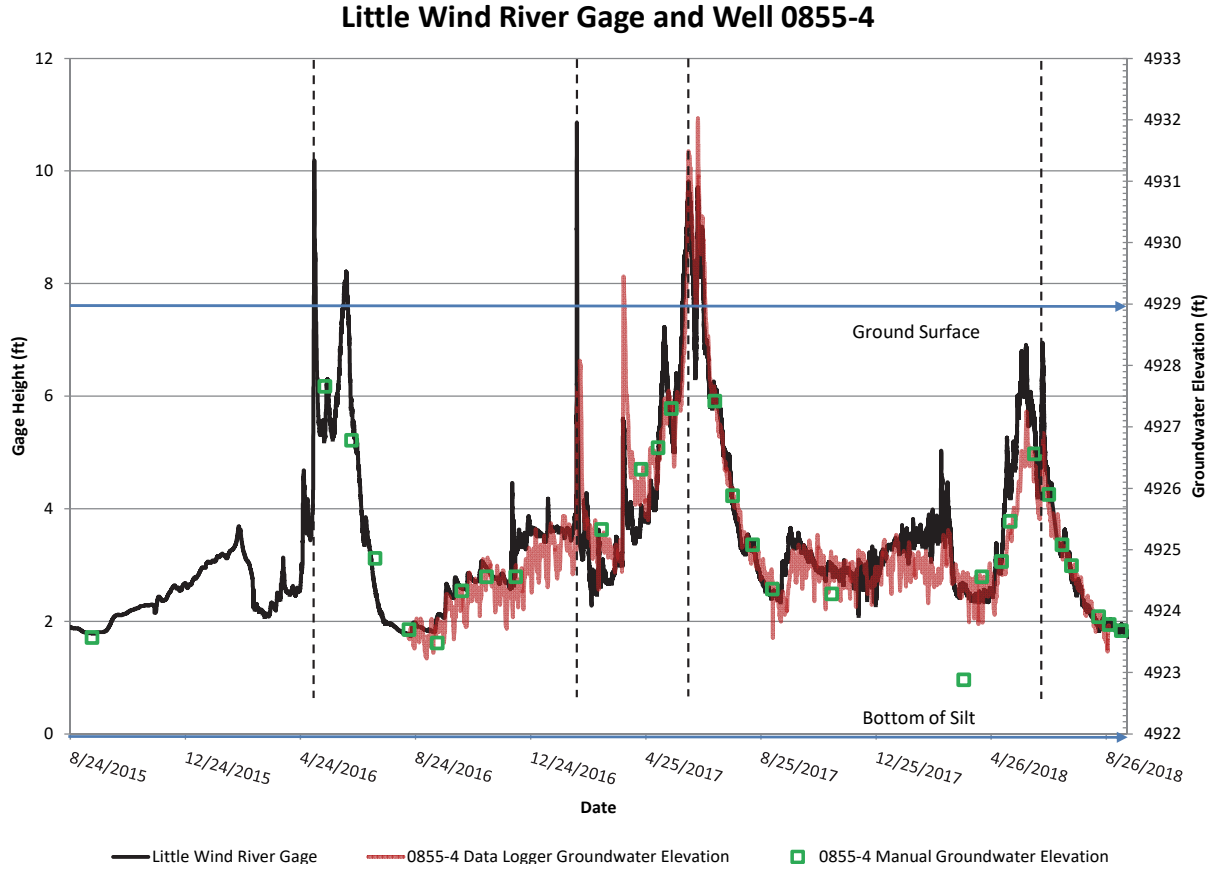

Figure 13. Well 0855 Hydrograph with Little Wind River Gage Heights

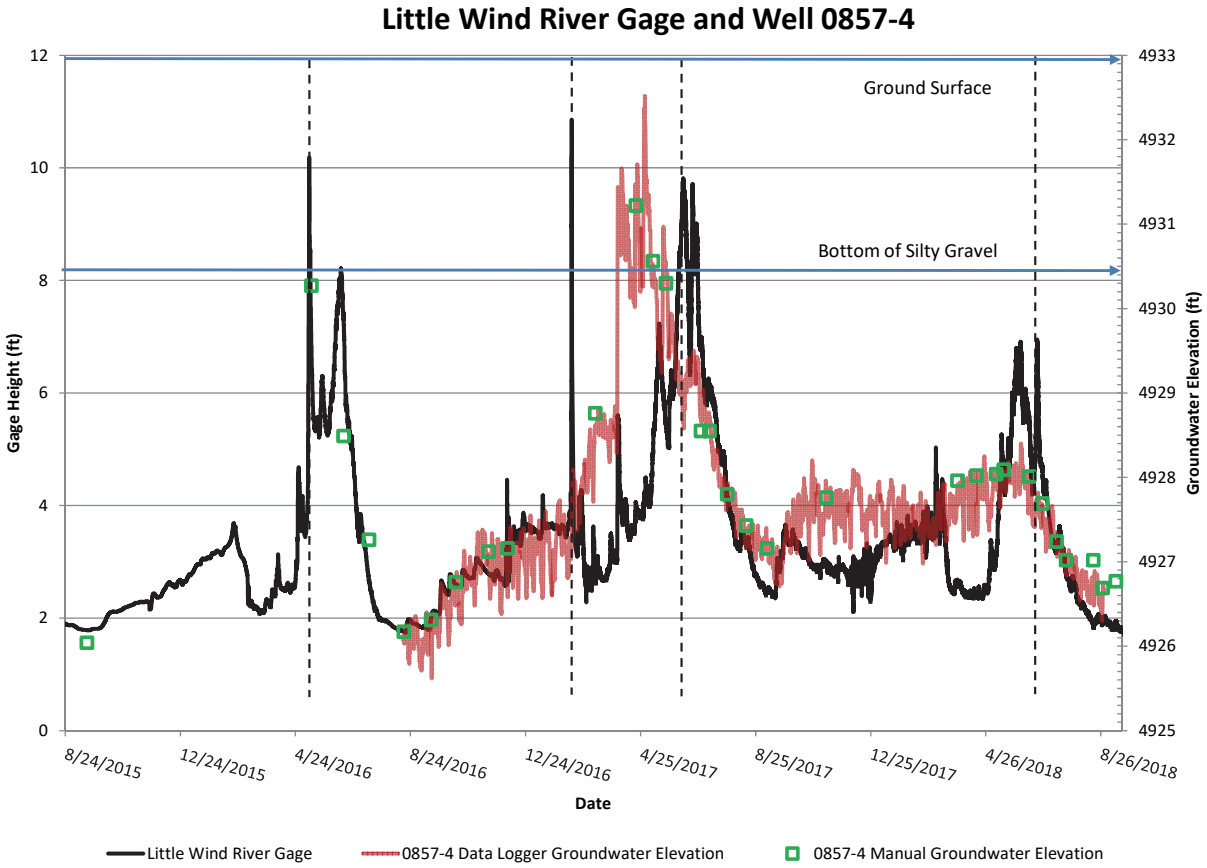

Figure 14. Well 0857 Hydrograph with Little Wind River Gage Heights

3.3 Geochemistry

Graphs of all of the geochemistry data for the multilevel wells are included in Appendix C. Data tables are provided in Appendix D (includes geochemistry data and manually measured water-level data). These graphs are ordered by well number and include constituent data in the following order: pH, alkalinity, calcium, magnesium, sodium, potassium, chloride, sulfate, iron, manganese, molybdenum, uranium, vanadium, silicon, and dissolved organic carbon. After the geochemistry data, PHREEQC results are graphed for each well in the following order: calcite ($CaCO_3$) saturation index (SI), dolomite (disordered) ($CaMg(CO_3)_2$) SI, magnesite ($MgCO_3$) SI, rhodochrosite ($MnCO_3$), carbon dioxide SI (equivalent to the log partial pressure of CO_2 in atmospheres (atm)), and gypsum ($CaSO_4 \cdot 2H_2O$) SI. An SI = 0 value means the mineral is in equilibrium with its associated dissolved constituents, whereas an SI < 0 value indicates that a mineral could be dissolved if it is present (undersaturated) and an SI > 0 value means mineral precipitation is a possibility (supersaturated). Reaction kinetics can slow down mineral dissolution and precipitation, but none of the minerals listed above should have any significant kinetic issues unless otherwise stated.

The PHREEQC results are used to determine the general geochemical conditions of the groundwater with respect to the above listed reactive minerals. General observations that are common to all of the multilevel wells are discussed first followed by highlights specific to each

well. Graphs for uranium and molybdenum are duplicated from Appendix C, since these are the contaminants of greatest interest. This report provides an interpretation of the most apparent geochemical changes in the multilevel wells over the three-year monitoring period. Additional geochemical interpretations, such as parameters for uranium reactions or statistical calculations of trends, are beyond the scope of this report.

3.3.1 Evaporites

The presence of high sulfate concentrations in surface evaporites is a natural process that occurs over and outside of the Riverton site contaminant plume (DOE 2014). In addition, other constituents that were measured in the multilevel wells (Mg, K, Na, Ca, SO_4, Cl, and DOC) were also found to be naturally concentrated in the silt layer. Visually, the presence of white evaporite flecks was confirmed in the silt layer both over and outside of the contaminant plume, and solid-phase concentrations of Mg, K, Na, Ca, SO_4, and Cl were high in the silt layer across the site (DOE 2016). Carbon concentrations were higher in the silt layer across the site as organic carbon and inorganic carbon, likely as calcite (DOE 2016). The presence of calcite in the silt layer has been confirmed by X-ray diffraction data (unpublished).

Generally, all the constituents above (Mg, K, Na, Ca, SO_4, Cl, and DOC) show spikes in concentrations in 2016 and 2017, but not in 2018 (Appendix C). Thus, these constituents appear to be released when flooding or large recharge events force water downward through the silt layer, thereby dissolving any evaporite minerals. This corresponds with the hydrologic events in 2016 and 2017 that did not occur in 2018. Concentration spikes are most evident for Mg, K, Na, SO_4, Cl, and DOC, with smaller spikes for Ca, which is likely controlled by both calcite and gypsum solubility. Calcite is almost always near equilibrium or supersaturated ($SI \geq 0$, Appendix C), and gypsum is generally near equilibrium or undersaturated ($SI \leq 0$, Appendix C). Gypsum and calcite have been identified in the three samples from the silt layer and range from 2 to 5.5 weight percent (unpublished data). Gypsum was also identified in a sample in the saturated zone below the former tailings pile, which is the likely initial source of high calcium and sulfate concentrations in the contaminant plume. Maximum magnesium concentrations may be controlled by dolomite and magnesite solubility limits, but the magnesite solubility limit is usually not reached; thus, dolomite is a more likely control (almost always near equilibrium or supersaturated). Sodium sulfate salts and sodium chloride solubility limits were always too high to be a controlling factor on these constituents. Slight differences in trends and possible mineral controls for each multilevel well are discussed in more detail in the sections below for each well (Sections 3.3.6 through 3.3.12).

Evaporites are likely formed in the silt layer from wicking and evapotranspiration of water from the underlying groundwater. This requires the groundwater table to be in contact with the bottom of the silt layer; thus, the reason the bottom of the silt layer in comparison with the water table was plotted in the prior figures and in Appendixes A and B.

3.3.2 Uranium and Molybdenum

Unlike constituents listed under evaporites in the section above, higher uranium and molybdenum concentrations in the solid phase do define the contaminant plume. Uranium and molybdenum are concentrated in the surficial evaporites (DOE 2014) and the silt layer over the contaminant plume (DOE 2016). Uranium concentration increases in 2016 and 2017 are apparent

in wells 0852 and 0855–0858. Trends in wells 0853 and 0854 for uranium are not as distinct. The uranium concentration spike in well 0852 is at a much lower concentration than in wells within the plume. Solid-phase uranium isotope data at well 0852 indicate the uranium at this location is not mill derived (unpublished data), although uranium concentrations in the groundwater do go above uranium standards for the site. Thus, naturally occurring uranium is concentrated in the silt across the site. However, solid-phase, mill-derived uranium is deposited in the silt at higher concentrations than background over the uranium plume (DOE 2014 and DOE 2016).

Molybdenum concentrations are near or below detection limits in wells 0852, 0853, and 0854 since they are at the edge or outside of the molybdenum plume (Figure 5). In the solid phase, molybdenum is found in very low concentrations in background samples compared to uranium concentrations (DOE 2016); thus, it is a unique indicator of being mill derived. Molybdenum concentrations do show distinct increases in 2016 and 2017 in wells 0856 and 0858, but trends in wells 0855 and 0857 are not as distinct.

Uranium and molybdenum concentrations in multilevel wells 0852–0858 appear to be consistent with contaminant release from evaporite dissolution in the silt layer. An additional control is likely sorption/desorption reactions in the silt and to a lesser extent in the underlying sand and gravel. No mineral controls were apparent in the PHREEQC simulations, but additional geochemical interpretations are beyond the scope of this report. More detailed discussions of uranium and molybdenum trends are provided on a well-by-well basis below (Sections 3.3.6 through 3.3.12).

3.3.3 Carbonate System

The carbonate system is mainly controlled by soil-gas carbon dioxide coupled with carbonate mineral dissolution to provide a near-neutral pH. Measured concentrations of alkalinity, calcium, and magnesium along with pH allow PHREEQC to provide calculations of carbon dioxide concentrations, along with the saturation indexes for calcite and dolomite. Values for pH are generally near neutral (pH close to 7) and range from 6.5 to 7.5, except for a few outliers, such as November 7, 2016, in well 0855 for all samples and June 5, 2017, in well 0858 for all samples. Similarly, alkalinity concentrations are generally in the range of 400–600 mg/L as $CaCO_3$. pH and alkalinity values are used by PHREEQC to compute carbon dioxide concentrations, which range from –1 to –2 log atm, with values that are generally close to –1.5 log atm. These values are typical for a groundwater system with recharge via percolation through soil, typically near –2 log atm compared with near –3.5 log atm for CO^2 in the atmosphere (Drever 1997). Note that with the log scale, typical groundwater systems have 32 times as much CO_2 as the atmosphere.

In reality, the soil-gas CO_2 is controlling the pH (more CO_2 lowers the pH), which in turn dissolves calcite, buffers the pH, and controls the alkalinity value. Given typical conditions, these reactions are not too variable. However, during the flooding and high recharge events of 2016 and 2017, a higher water table may have provided more soil moisture with more carbon oxidation (and thus higher soil-gas CO_2 concentrations) than occurs with dry sediment. This influence is subtle, but can be seen as an alkalinity increase after the flood in May 2016 and the high water tables and flood in the spring of 2017, especially in the shallow ports of wells 0856 and 0858 (Appendix C). Compared with the large changes in sodium, chloride, and sulfate after

flooding events, the pH, alkalinity, and carbon dioxide variations through time are smaller (Appendix C) due to controls by the carbonate reaction system.

3.3.4 Manganese and Iron

Manganese is generally near 1 to 2 mg/L, which indicates groundwater that is slightly reducing, as manganese oxides are not very soluble in the presence of oxygen. This is consistent with dissolved oxygen measurements that are often less than 1 mg/L (Appendix D). Manganese can highlight subtle redox variations with depth, like the well port 0855-4 condition being more reducing than the well port 0855-3 condition, which is in turn more reducing than 0855-2, as manganese concentrations consistently increase with depth (Appendix C). In addition, when the shallow ports (e.g., 0857-1 and 0858-1) become saturated and remain saturated (spring of 2017), increasing manganese concentrations are consistent with the increasing alkalinity values associated with carbon dioxide production and calcite dissolution (created by the high water table and onset of more reducing conditions). Rhodochrosite ($MnCO_3$) is a likely control on the upper limit of manganese. Rhodochrosite is generally near equilibrium or slightly supersaturated for wells 0852–0854 and near equilibrium or slightly undersaturated for wells 0855–0858, except for the high manganese concentrations in 0858-1 and supersaturated rhodochrosite during the late spring of 2017.

Similar to manganese, iron concentrations also indicate slightly reducing conditions, with concentrations generally ranging from 0 to 3 mg/L. Iron oxides are sparingly soluble in the presence of oxygen, and the variability in iron concentration through time is likely controlled by recharge events that bring oxygenated water to the shallow aquifer. Dissolved oxygen concentrations are provided in Appendix D, but not plotted, as these measurements are not considered reliable enough for determining detailed trends. Shallow ports (e.g., 0857-1 and 0858-1) show the similar onset of increasing iron concentration in the spring 2017 with 0857-1 reaching a concentration of 30 mg/L iron on June 21, 2017. Iron concentrations in well 0855 do not show the same trend as manganese, as the lowest iron concentrations are consistently in port 0855-3.

3.3.5 Silicon and Vanadium

Silicon was measured to be available in later evaluations that might include the evaporation of unsaturated zone water to uranium minerals such as soddyite ($(UO_2)2SiO_4 \cdot 2H_2O$). Vanadium was included for later evaluations of uranium minerals such as carnotite ($K_2(UO_2)_2(VO_4)_2 \cdot 3H_2O$). However, vanadium was never above the analytical detection limits (Appendix C).

3.3.6 Well 0852

Well 0852 is outside the mill-derived molybdenum and uranium plumes (DOE 2016). Molybdenum at this location is generally not detectable, except for the September 2015 sample with lower detection limits (Figure 15). However, uranium does spike to concentrations above the Riverton site standard of 0.044 mg/L uranium in groundwater (Figure 16), and in Figure 4, well 0852 appears to be within the mill-related uranium plume. However, data indicate that uranium is naturally concentrated in a silt layer due to evaporite formation and uranium in the groundwater at this location is naturally occurring (DOE 2016). After the flooding event in

May 2016, uranium concentrations increased to above the site standard, especially in ports 1 and 2. A similar spike in uranium occurred in 2017, but no spike occurred in 2018, a year without any flooding, and uranium concentrations have since decreased to below the uranium standard (Figure 16).

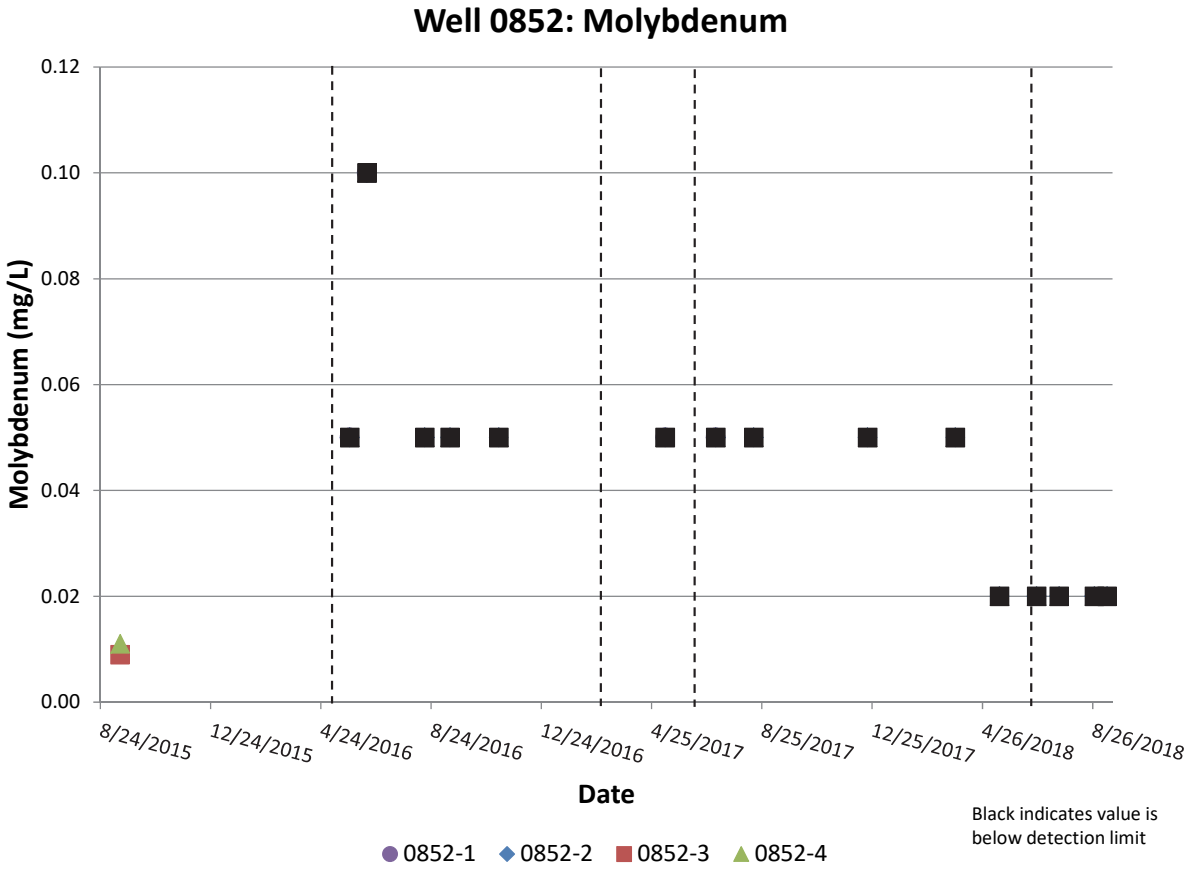

Figure 15. Multilevel Well 0852 Molybdenum Concentrations

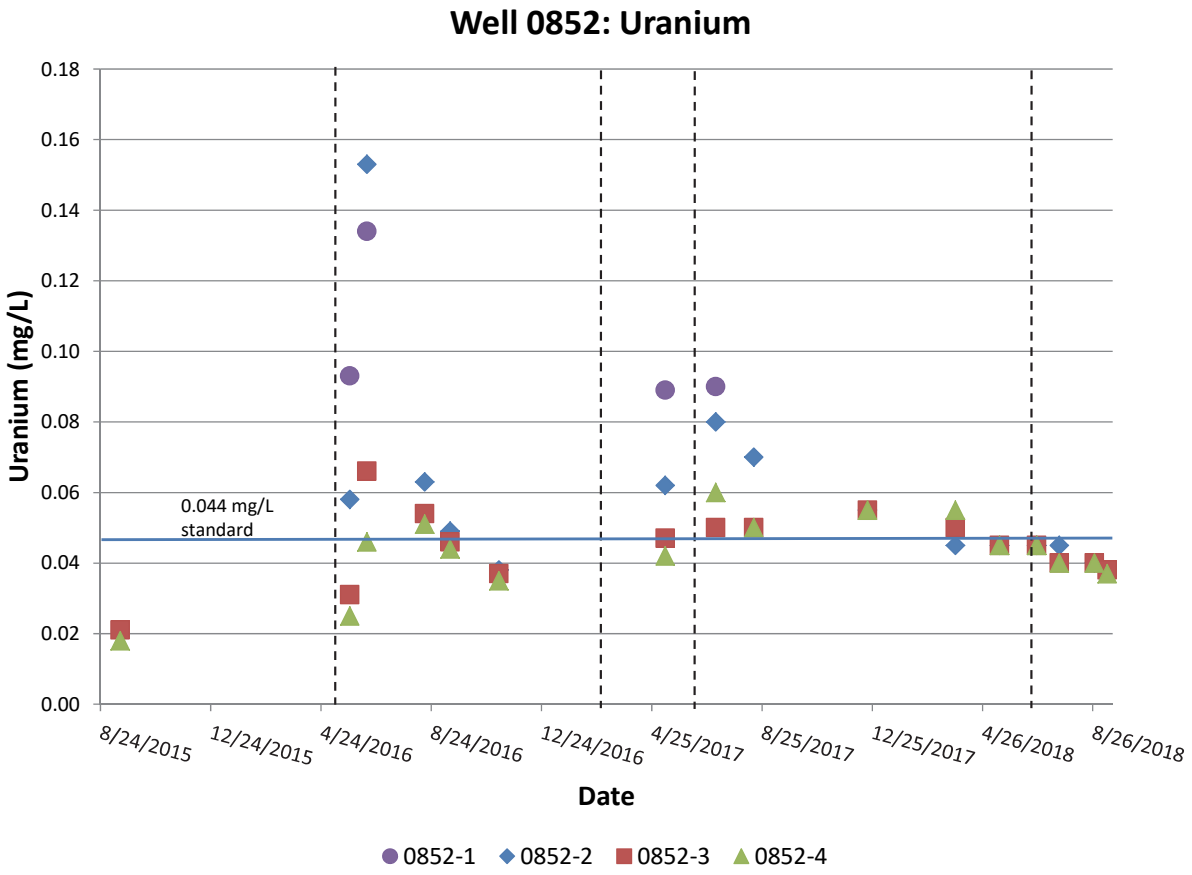

Figure 16. Multilevel Well 0852 Uranium Concentrations

Other constituents have trends similar (Appendix C) to those of uranium, with concentration spikes after the May 2016 and June 2017 flooding events, with no concentration spikes in 2018. In addition, the high recharge in the spring of 2017 creates a release of constituents to ports 1 and 2 in May 2017, before the June 2017 flooding. In 2016 and 2017, concentration increases in the bottom two ports appear to be delayed by several weeks after the spring flooding events in these two years. These trends are especially apparent for sodium, sulfate, and chloride (Appendix C), which are likely present in the silt layer evaporites that are dissolved when large recharge events occur. Sodium and chloride increases are as great as in some of the multilevel wells within the contaminant plume.

From the PHREEQC simulations, the carbonate minerals calcite, dolomite, rhodochrosite are all at equilibrium (SI = 0) or supersaturated (SI > 0), which likely controls the maximum concentrations of calcium, magnesium, and manganese. Gypsum is generally undersaturated (SI < 0), which is consistent with this well not being directly downgradient from the former tailings pile (Figure 6).

3.3.7 Well 0853

Well 0853 is outside the mill-derived molybdenum plume (Figure 5) and at the edge of the uranium plume (Figure 4). Molybdenum concentrations are generally at or near detection limits (Figure 17).

Uranium shows a significant concentration spike in ports 2 and 3 with uranium concentrations exceeding the 0.044 mg/L standard after the 2016 flood event. All ports did not exceed the standard in 2015 (Figure 18). Uranium concentrations in port 4 did not change much on May 27, 2016, after the May 8, 2016, flood event. With the later sampling in 2016, all ports (2, 3, and 4) remained above the uranium standard (port 1 has never been saturated). Uranium concentration trends beyond August 2016 are not readily apparent (Figure 18).

Some concentration increases in other constituents occur after the 2016 and 2017 flooding events, but are most evident for sulfate and chloride, especially in 2017 (Appendix C). The hydrograph for well 0853 (Appendix B) does not indicate flooding above ground surface, but this was due to access issues, as the ground surface at 0853 did flood and it was not accessible for manual water-level measurement.

In the PHREEQC analysis, it is notable that gypsum was undersaturated in 2015 and at or nearly saturated in all ports after the May 8, 2016, flood event, except for port 4 on May 27, 2016, due to a lag in calcium and sulfate concentration increases.

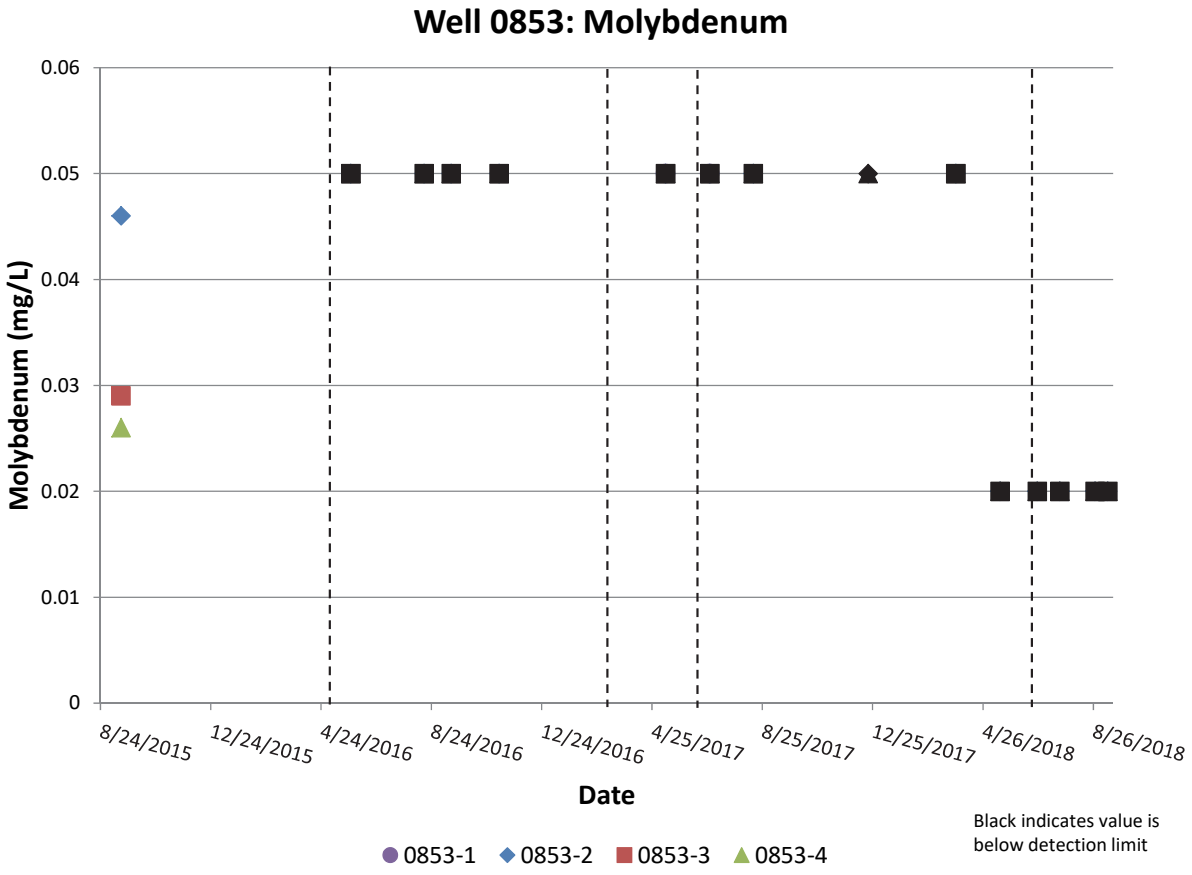

Figure 17. Multilevel Well 0853 Molybdenum Concentrations

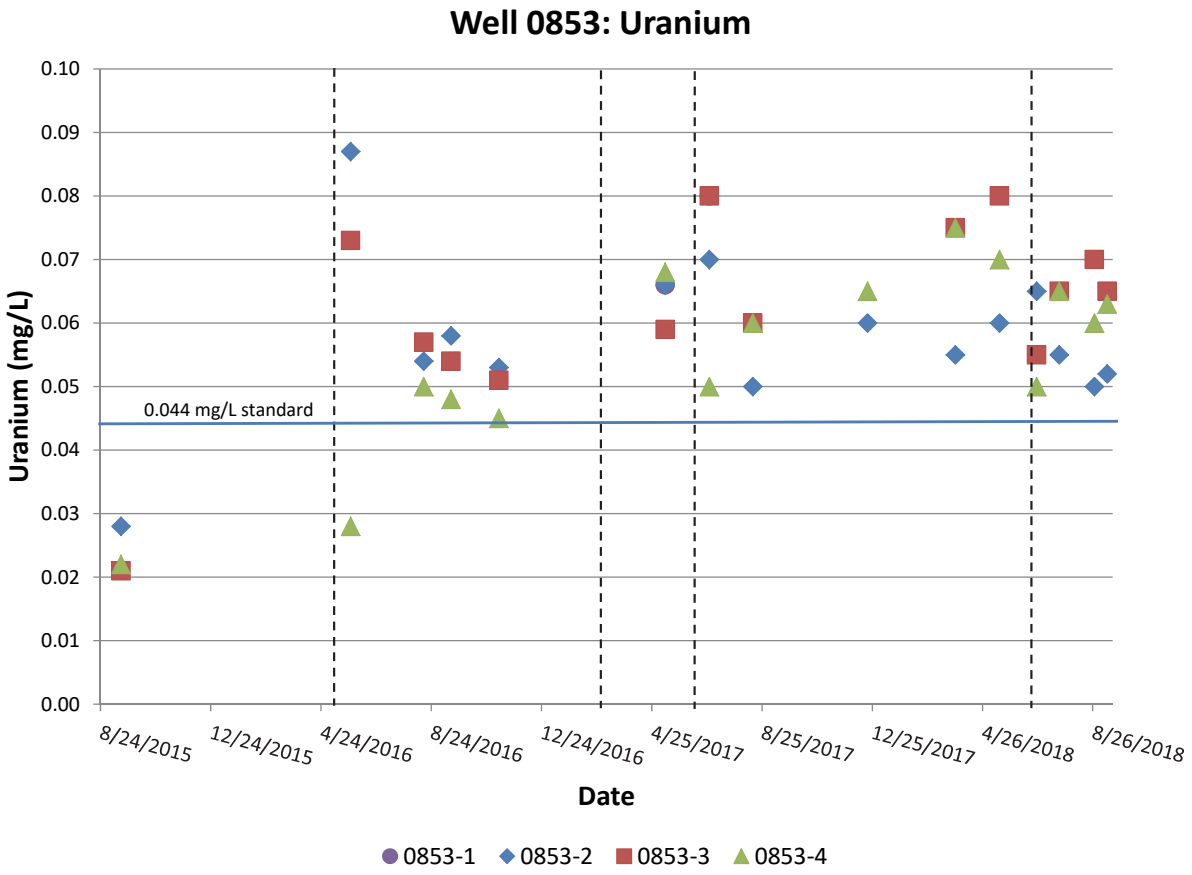

Figure 18. Multilevel Well 0853 Uranium Concentrations

3.3.8 Well 0854

Well 0854 was at the edge of the flooded zone during the monitoring time period, and measured groundwater elevations were less than 1.3 ft below the ground surface. In 2015, molybdenum and uranium concentrations in well 0854 were slightly greater than those in well 0853. Molybdenum concentrations were just barely above detection limits (Figure 19). Uranium concentrations were near the 0.044 mg/L standard in 2015, increased post-flood in 2016, and remained above the standard in 2017 and 2018 (Figure 19). Port 1, when it became saturated with the high water table in 2017, had the highest concentrations recorded for K, Mg, alkalinity, Mo, Na, U, SO_4, Cl, and DOC. Many of these same constituents increased slightly in concentrations from 2015 to 2016, but in 2017, ports 2, 3, and 4 do not increase in concentration like port 1 (Figure 19, Figure 20, and Appendix C). This likely indicates that evaporite-related constituents in the silt were released to the top of the water table and a significant portion of the dissolved constituents did not reach the lower portions of the aquifer until later. Ports 2, 3, and 4 maintained higher concentrations of the above constituents in 2016 and 2017 than in 2015, with stable or slightly decreasing concentrations in 2018, except for a slight increase in alkalinity in 2018, along with manganese. Gypsum is near or undersaturated in the three-year monitoring period (Appendix C) since it has lower sulfate concentrations than in wells 0855–0858.

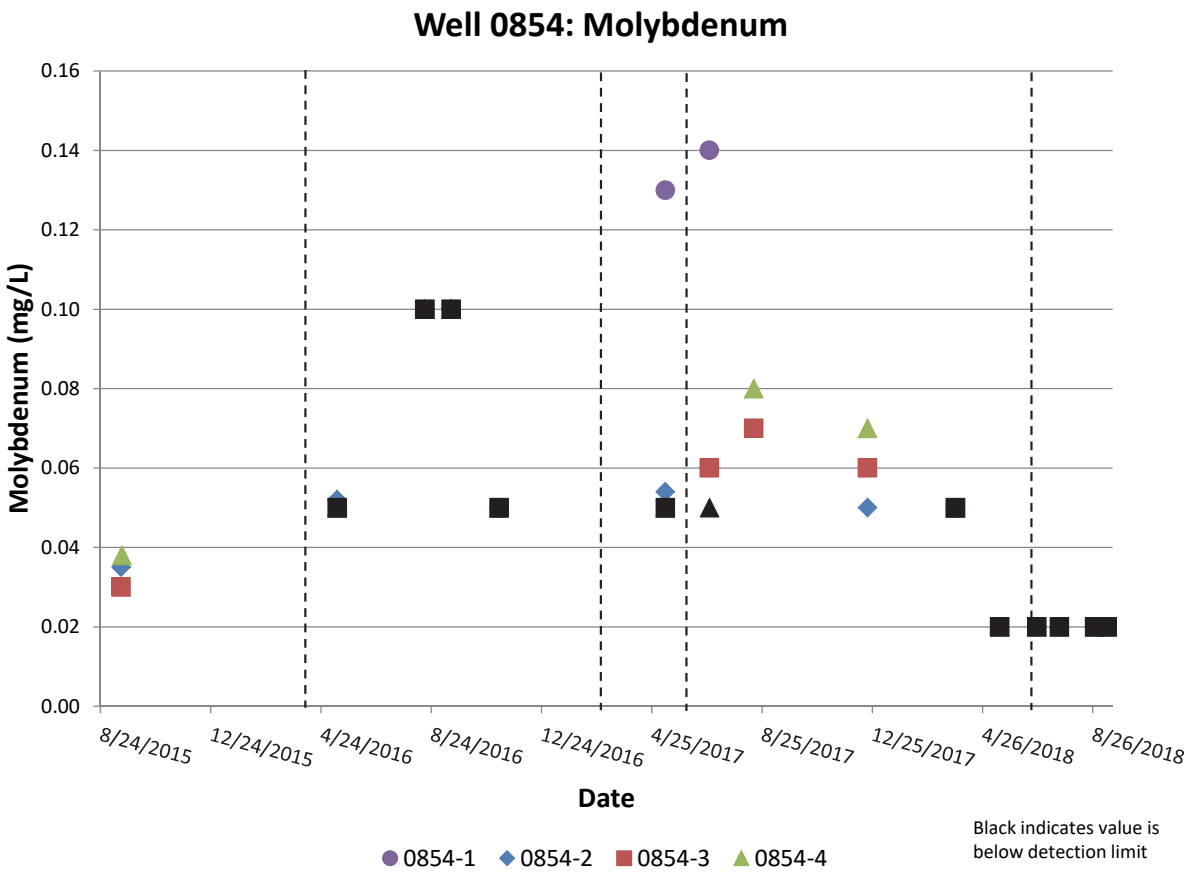

Figure 19. Multilevel Well 0854 Molybdenum Concentrations

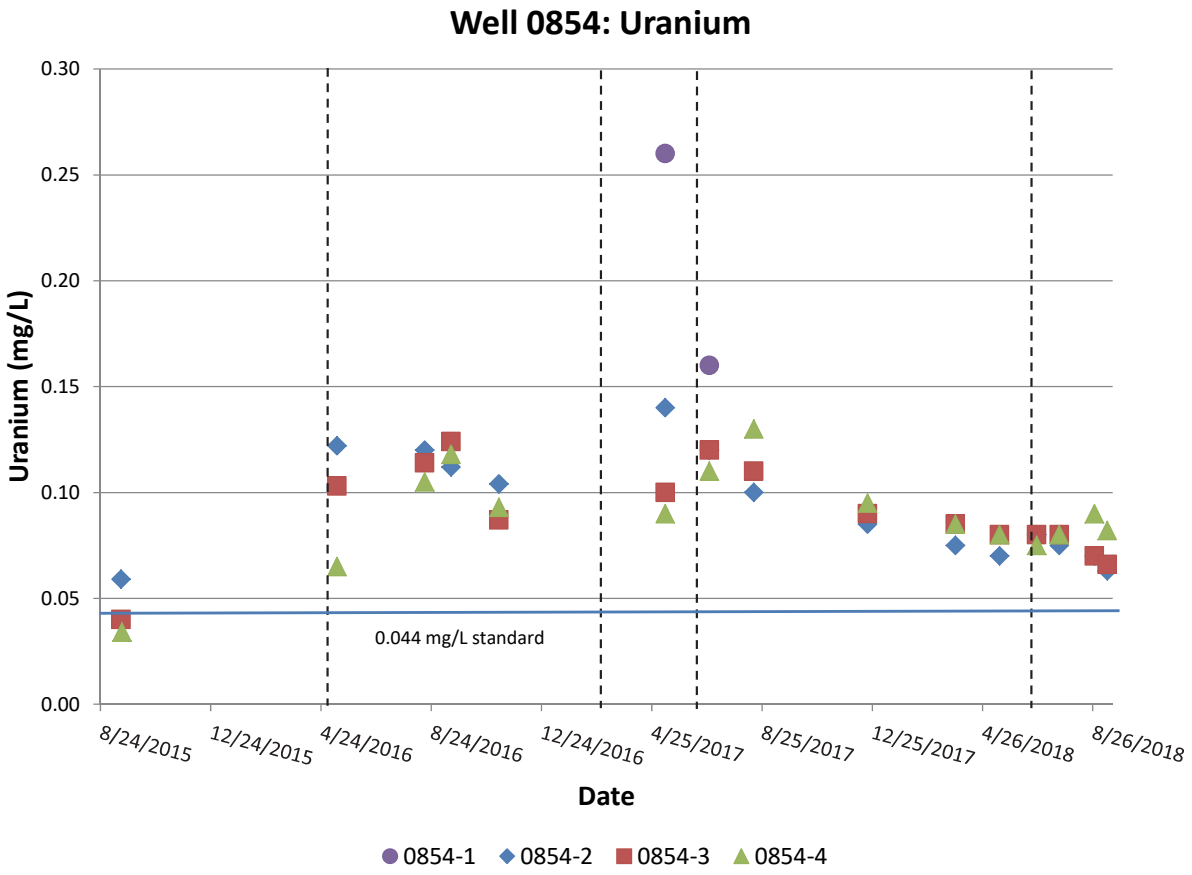

Figure 20. Multilevel Well 0854 Uranium Concentrations

3.3.9 Well 0855

Molybdenum concentrations in well 0855 do not show any distinct trends (Figure 21). Uranium concentration trends are subtle, but follow an overall pattern of increasing concentrations from 2015 to 2016 continuing into 2017. In 2018, concentrations appear to have remained stable and uranium in port 4 remains lower in concentration than in the other ports throughout the monitoring period (Figure 22). Notable uranium concentration changes are a spike in uranium for ports 1 and 2 after the May 2016 flood event. The higher recharge in early 2017 creates uranium concentration increases in ports 2 and 3. For reference, port 1 is in the typically unsaturated silt, port 2 is in the shallow aquifer just below a high organic, saturated silt, port 3 is in the middle of the sand and gravel aquifer, and port 4 is at the bottom of the aquifer (DOE 2016).

Other evaporite-related constituents (e.g., Mg, Na, SO_4, and Cl) show trends similar to that of uranium. In addition, these additional constituents highlight higher concentrations in the summer of 2016 in ports 2 and 3 that are followed by a slight decline. Similar to uranium, these constituents reach peak concentration in ports 2 and 3 in the summer of 2017 with a slight decline followed by relatively stable concentrations in 2018. Port 4 is lower in concentration than ports 2 and 3 for these constituents (including uranium), with a slow, steady rise in concentrations from 2015 through 2017, followed by stable concentrations throughout 2018 (Appendix C and Figure 22).

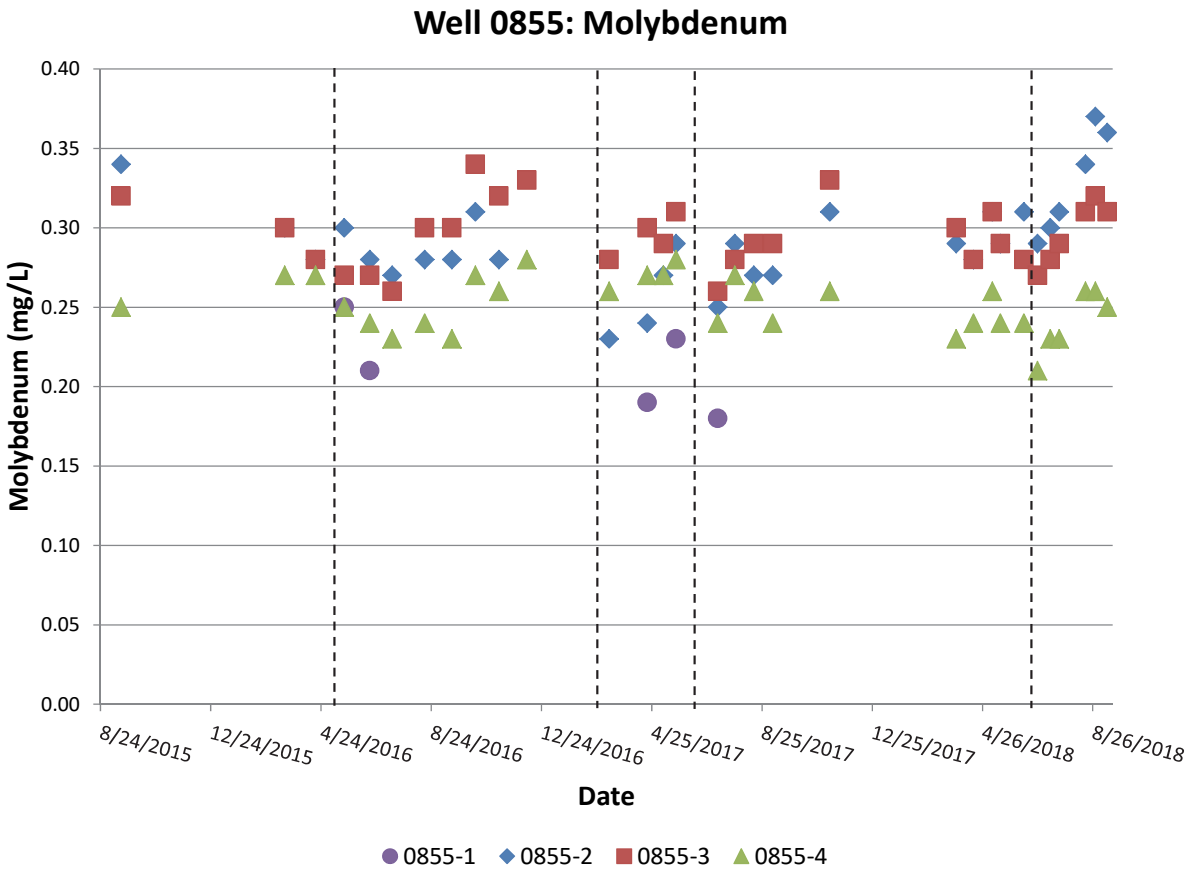

Figure 21. Multilevel Well 0855 Molybdenum Concentrations

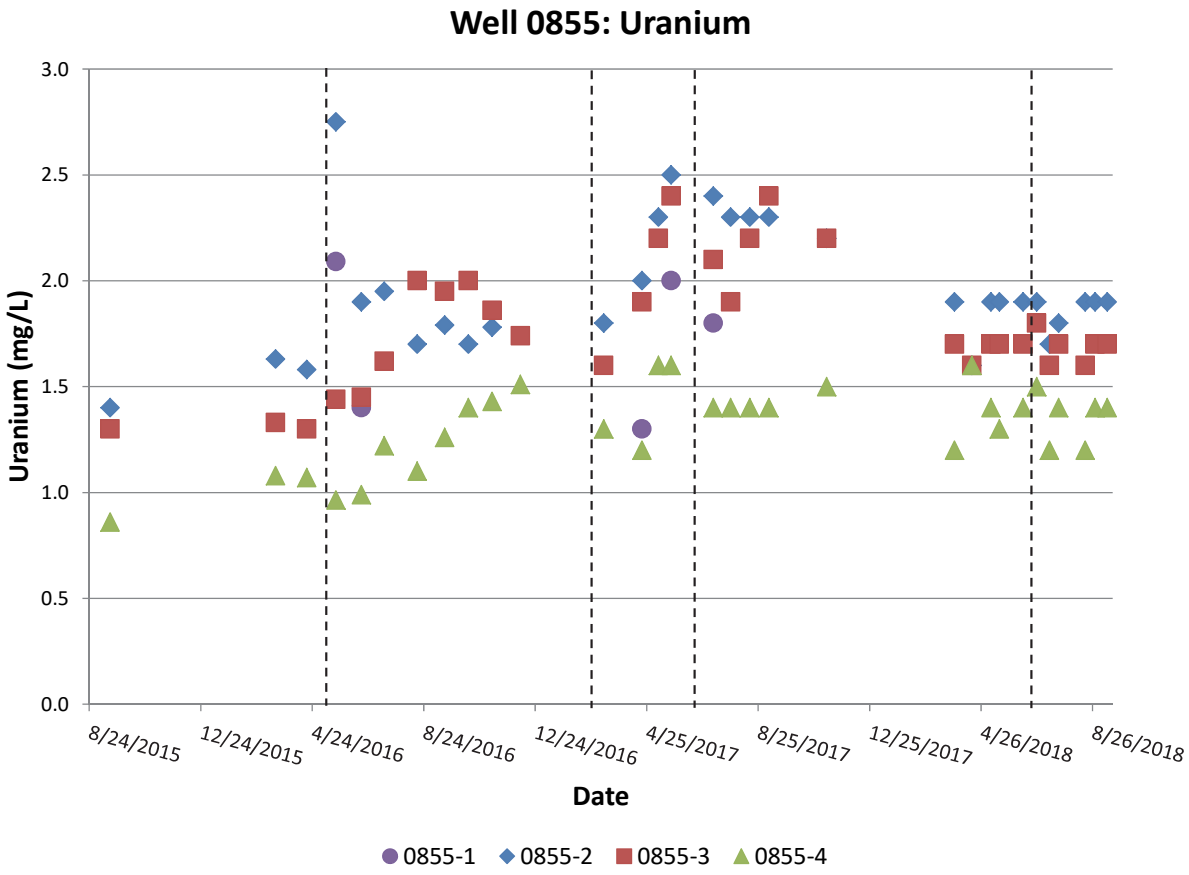

Figure 22. Multilevel Well 0855 Uranium Concentrations

For manganese, port 4 has the highest concentration, followed by port 3, and then port 2 (Appendix C). This implies that port 4 is more reducing, but it is not clear if this controls uranium concentrations more than the inflow of upgradient groundwater (well 0856). Iron is more difficult to interpret for ports 2 and 4, but port 3 has less iron. Calcium and alkalinity show subtle increasing trends from 2015 through 2017, likely controlled by carbonate minerals such as calcite. Gypsum is generally near saturation or supersaturated (Appendix C).

3.3.10 Well 0856

Of all the multilevel wells, 0856 shows the most dramatic increases in evaporite-related constituents (K, Mg, Na, SO_4, and Cl, plus DOC) in 2016 and 2017. Peak concentrations of these constituents, along with molybdenum and uranium, occurred in July and August of 2016 and May through September of 2017 (Figure 23, Figure 24, and Appendix C). Well 0856 experienced flooding conditions at the surface in May of 2016 and June of 2017.

The highest concentrations of most constituents (except Fe, alkalinity, and Ca) occurred on August 16, 2016, in port 4. It is likely that flow through the silt occurred near well 0856 during the May 8, 2016, flood, creating an initial increase in these constituents (Figure 23, Figure 24, and Appendix C), but upgradient infiltration through silt with high evaporite concentrations created density-driven flow with a delay in reaching 0856-4.

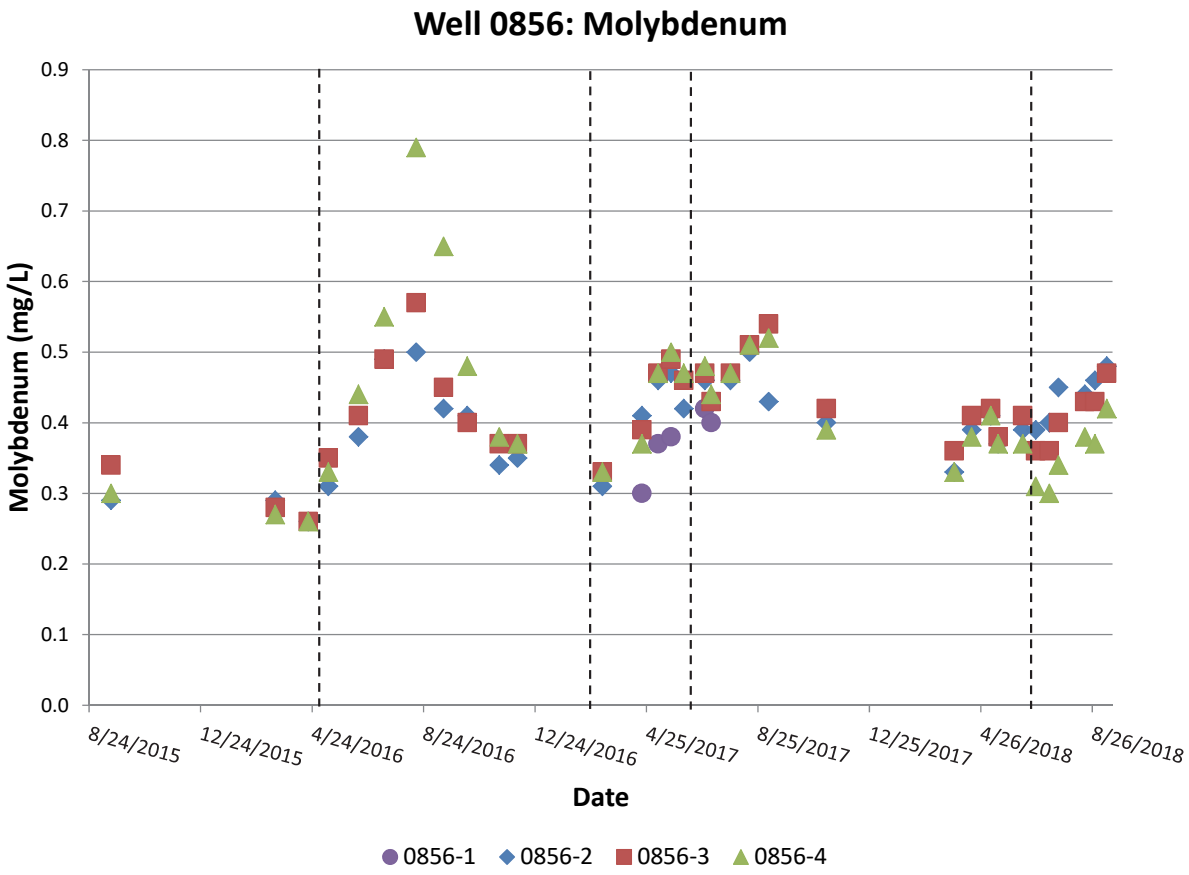

Figure 23. Multilevel Well 0856 Molybdenum Concentrations

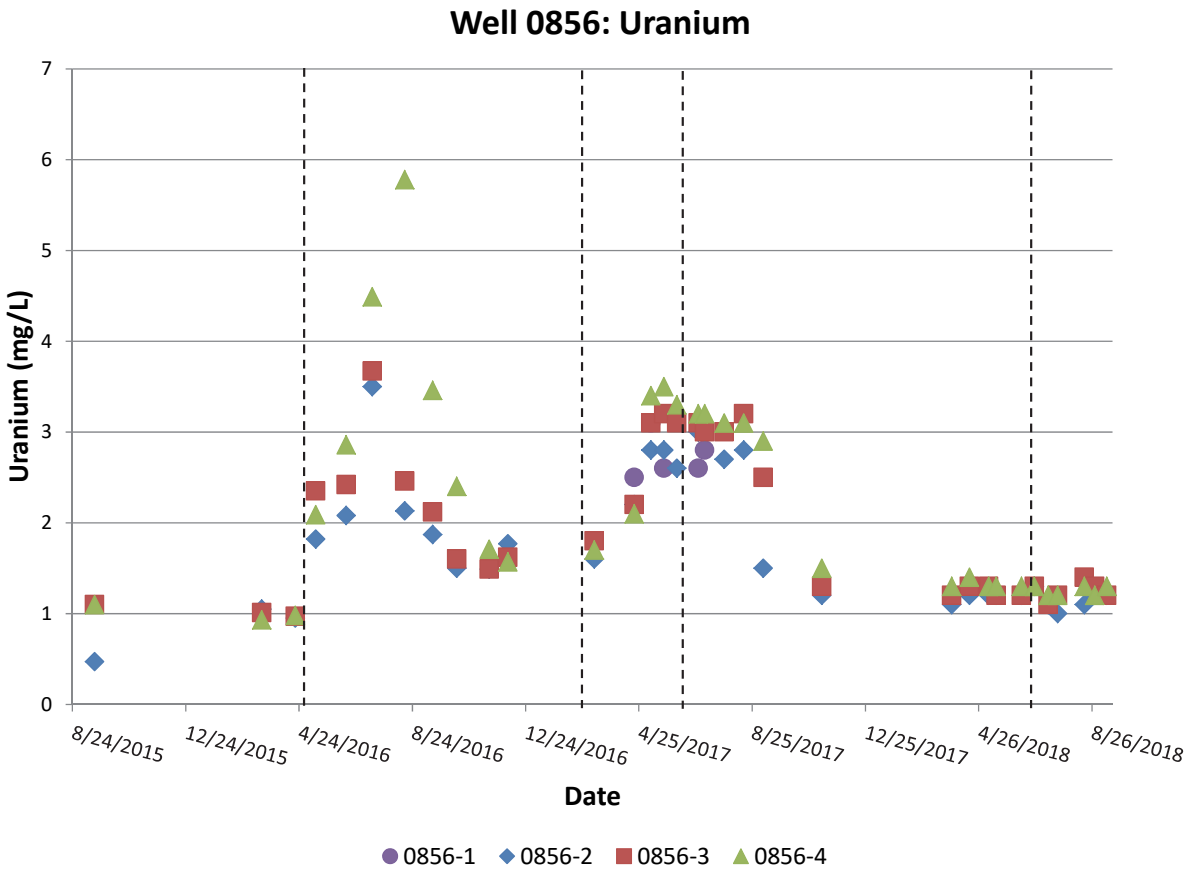

Figure 24. Multilevel Well 0856 Uranium Concentrations

A similar increase in evaporite-related constituents occurred in the spring of 2017 due to a large amount of recharge through the silt layer, but this event did not create the large delayed concentration spike in port 4. In addition, this event created high concentrations in port 1 associated with the high water table in April 2017 through July 2017. Overall, the June 2017 flooding did not create additional concentration spikes, but may have helped maintain higher concentrations for a longer time period.

Gypsum is generally near equilibrium or slightly supersaturated (Appendix C) and appears to be controlled mainly by calcium concentrations. Calcium is in turn controlled by calcite, which is generally supersaturated (except for a few data points in the spring of 2017 due to low pH measurements, which may have been due to measurement error, given the extremely low values). Gypsum supersaturation (SI of 0.10–0.15) is more apparent in 0856-2 in the spring of 2017 when calcium concentrations are higher than in the other ports.

3.3.11 Well 0857

The borehole log for well 0857 (DOE 2016) indicates this is the only multilevel well location without a distinct silt layer, and the log shows silty gravel from the water table to the ground surface. This geology couples with evaporite-type constituents (K, Mg, Na, Ca, SO_4, and Cl) that do not spike in concentrations immediately after the May 8, 2016, flood, but do slowly increase

that year with peak concentrations in August and September 2016 (Appendix C). Likewise in 2017, these constituents increase throughout the spring and level off at near peak concentrations around August (Appendix C). However, in 0857-1 and to a lesser amount in 0857-2, these same constituents have lower concentrations than in 0857-3 and 0857-4, especially for sulfate and chloride. This is likely due to the lack of a distinct silt layer that can concentrate evaporites. As such, these constituents are probably less concentrated in the shallow subsurface near well 0857 and concentrations increase at this well later in ports 3 and 4, as the silt layer is likely present nearby. Concentrations of these evaporite-type constituents remain relatively constant in 2018.

In the spring of 2017, well port 0857-1 shows dramatic increases in manganese, iron, and molybdenum with a decrease in uranium. Similar trends are also seen in 0857-2 (Appendix C, Figure 25, and Figure 26). This suggests that reducing conditions were likely during the high water tables in the spring of 2017, with an associated release of manganese and iron. In addition, it appears that molybdenum may be associated with the iron or manganese, but not uranium. Uranium may occur in lower concentrations at this location due to the lack of a distinct silt layer, or uranium may sorb more strongly to the sediment under more reducing conditions. The onset of reducing conditions is coupled with dramatically increasing dissolved organic carbon concentration along with greater alkalinity and carbon dioxide concentrations (Appendix C). These data make sense with the prior discussions that oxidation of organics produces more carbon dioxide, which in turn dissolves more carbonates due to the added acidity. The pH values remain near neutral but decrease slightly in the summer of 2017 (Appendix C). Uranium appears to follow the evaporite-type constituent trends for 0857-3 and 0857-4 (Figure 26).

Given the onset of reducing conditions described above, manganese is likely controlled by rhodochrosite solubility. Likewise, Ca and Mg are likely controlled by calcite and dolomite ($CaMg(CO_3)_2$) solubility, which remain supersaturated. Gypsum remains near equilibrium or supersaturated (except for 0857-1 with low Ca concentration, undersaturated with respect to gypsum) with saturation trends that appear to be controlled mainly by calcium concentrations (Appendix C). It is unusual to see the large changes in calcium concentrations along with gypsum being supersaturated up to an SI of 0.27, as gypsum is typically a reactive mineral that reaches equilibrium concentrations relatively quickly. However, gypsum precipitation may be inhibited in this case, due to the high concentration of dissolved constituents, including magnesium (Ahmed et al. 2014).

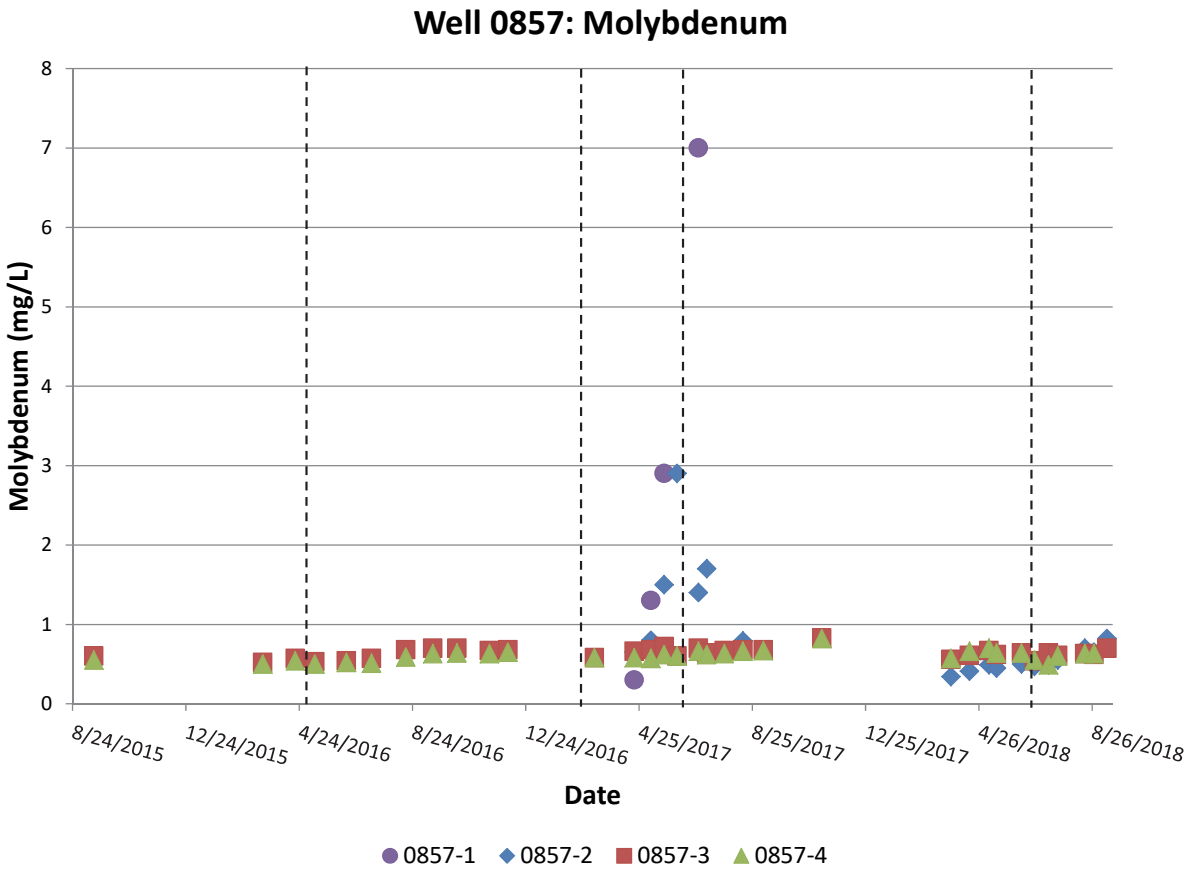

Figure 25. Multilevel Well 0857 Molybdenum Concentrations

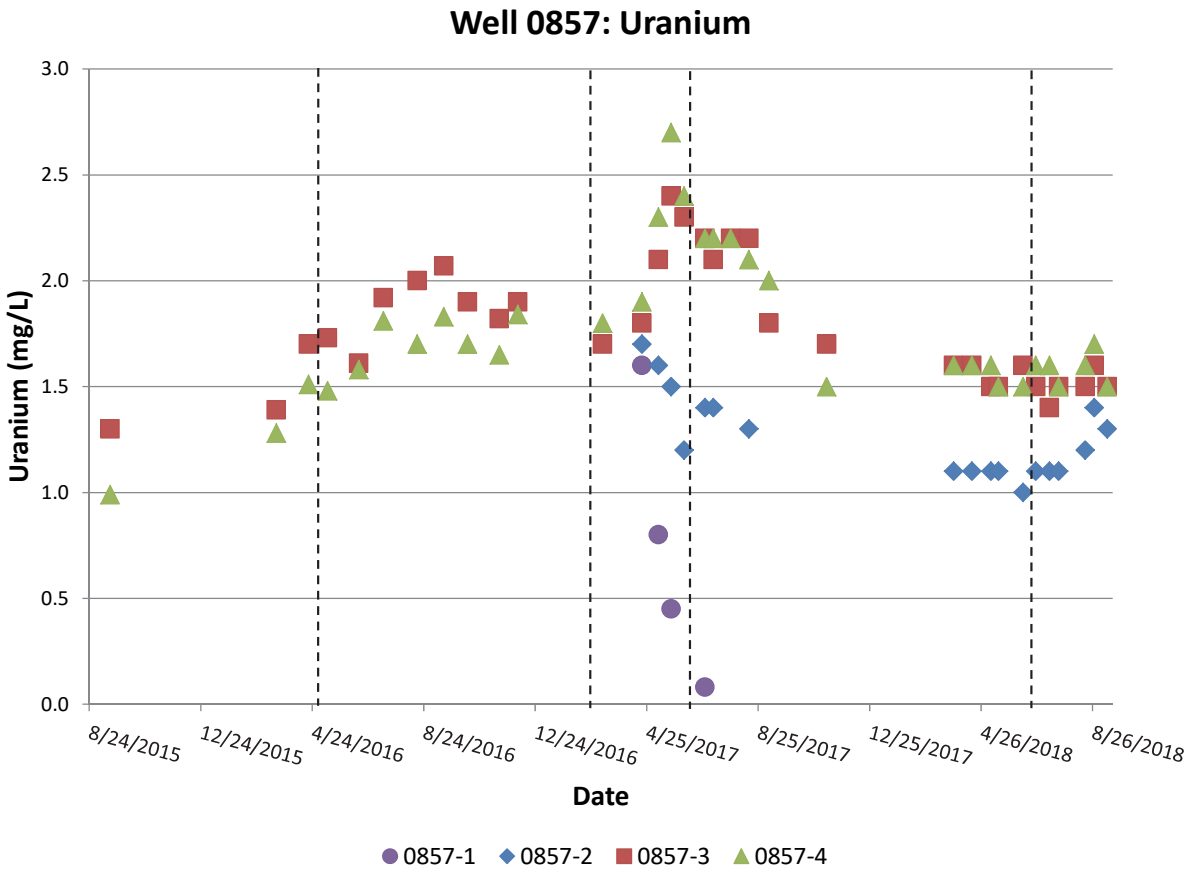

Figure 26. Multilevel Well 0857 Uranium Concentrations

3.3.12 Well 0858

Evaporite-type constituents (K, Mg, Na, Ca, SO_4, and Cl) spike in concentration immediately after the May 8, 2016, flood in well 0858 ports 1 and 2. Ports 3 and 4 increase dramatically in these constituents with the next sampling event on June 15, 2016 (Appendix C). These data are consistent with the presence of a silt layer at this well and high concentrations of evaporites in the shallow subsurface (DOE 2016) that are released during a flooding event. The same increases for these constituents occur in 2017, but port 1 tends to have lower concentrations, which may indicate that more than one year is necessary to fully reconcentrate the evaporites. In addition, the overall 2017 concentration increases occur steadily with a peak in July 2017 after the June 2017 flooding event. In 2018, these constituent concentrations stayed relatively the same (Appendix C).

Trends similar to those of the evaporite-type constituents are seen for molybdenum (Figure 27) and uranium (Figure 28). Port 1 shows similar trends for manganese, iron, molybdenum, and uranium as well 0857 with a possible onset of reducing conditions and similar mechanisms as discussed for 0857. The increase in alkalinity, carbon dioxide, and dissolved organic carbon concentrations for well 0858 also suggest the onset of reducing conditions with the high spring 2017 water table. However, at well 0858 the presence of evaporites in the silt layer that are high in molybdenum and uranium (DOE 2016) may provide a greater control on these elements than redox controls.

Similar to the well 0857 case, rhodochrosite is a likely control on manganese concentration and calcite and dolomite are likely controls on calcium and magnesium. Dolomite is near equilibrium, and calcite is generally supersaturated (SI near 0.4). Gypsum was undersaturated before the May 2016 flood, but has remained near equilibrium or supersaturated since that time, reaching a peak SI of 0.29 in July 2016. Gypsum saturation appears to be strongly controlled by the calcium concentration (Appendix C), and precipitation may be inhibited by the mechanism as discussed for 0857.

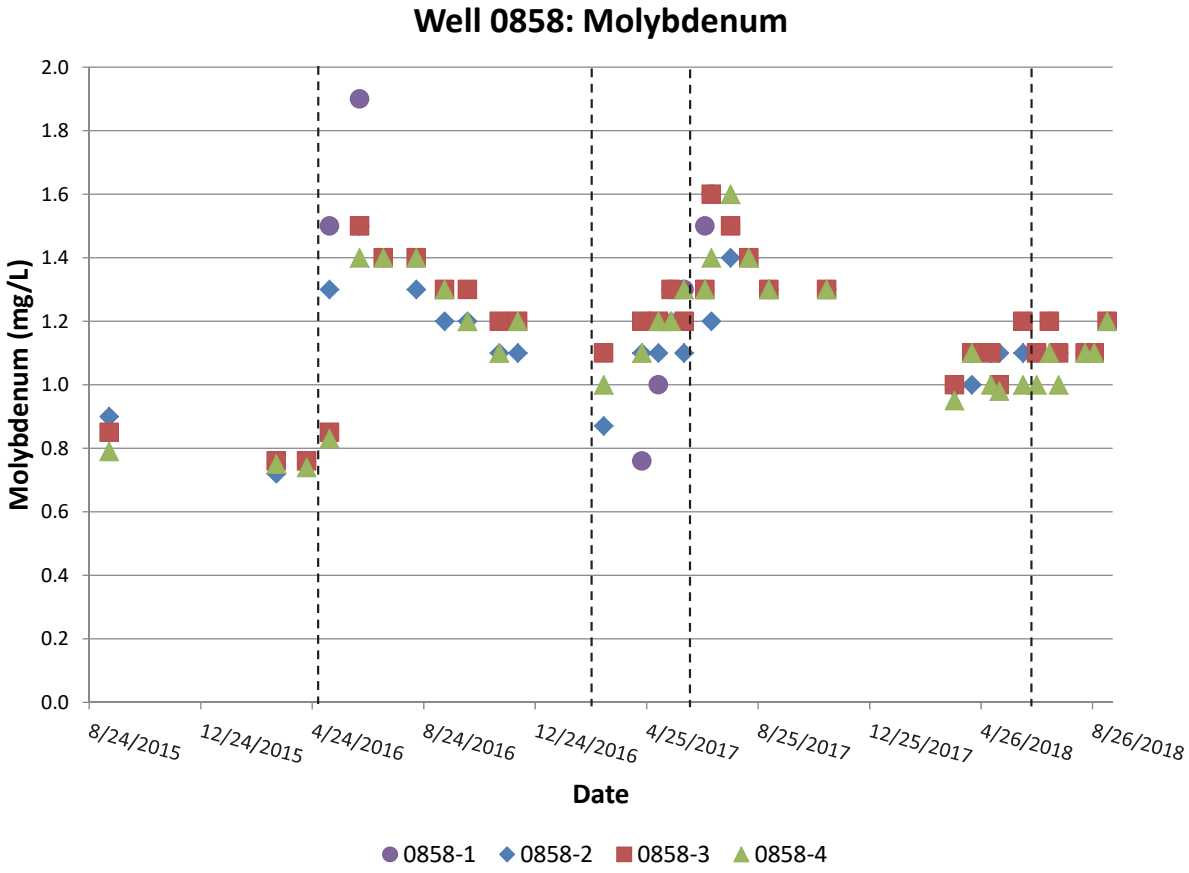

Figure 27. Multilevel Well 0858 Molybdenum Concentrations

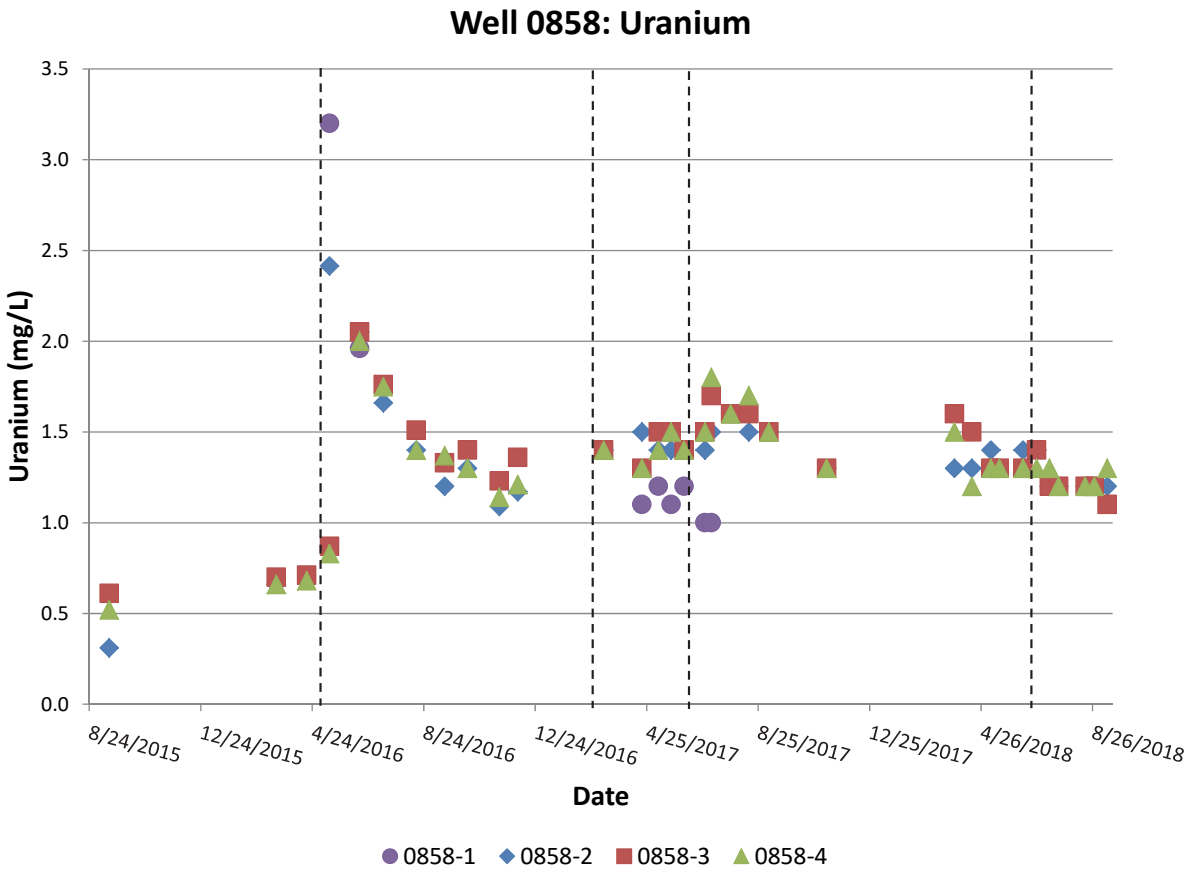

Figure 28. Multilevel Well 0858 Uranium Concentrations

4.0 Summary

Past reports (DOE 2014 and DOE 2016) indicated higher concentrations of solid-phase uranium and molybdenum in evaporites above the respective contaminant groundwater plumes. Given these data, multilevel monitoring wells were installed in 2015 to monitor seasonal changes in groundwater quality. Data from three years of monitoring are summarized in this report. The results indicate that evaporite-related constituents (especially Na, SO_4, and Cl) present across the site in a silt layer can be released to the shallow sand and gravel aquifer during flooding and large recharge events. The solid-phase and water-phase data confirm that these evaporites are mainly sodium sulfate and sodium chloride salts with some calcite and gypsum.

The Riverton site underwent flooding near the Little Wind River in early May 2016, February 2017, and June 2017. The May 2016 flooding was due to a large rain. The February 2017 flooding was due to an ice jam, and the June 2017 flooding was due to mountain snowmelt runoff. In addition, the site exhibited high water tables in April and May 2017, as this was the second wettest spring in Riverton, Wyoming, since records began in 1918. All of these events likely created downward flow through the silt layer that enhanced dissolution and transport of constituent in the evaporites. Depending on the amount of silt and evaporites near each respective well, these constituents either increase immediately at the top of the aquifer after an extreme event or have delayed increases in the aquifer due to nearby dissolution. A well

outside of the contaminant plume (0852) confirms that the formation of evaporites and subsequent release of evaporite-related constituents to the shallow groundwater is a naturally occurring process. Flooding or extreme recharge did not occur in 2018, and the groundwater quality remained relatively unchanged in that year. Thus, release of evaporite-related constituents appears to require downward flow through the typically unsaturated zone and does not occur with seasonally high water tables.

Uranium and molybdenum can be concentrated in the evaporites within the silt at the Riverton site (DOE 2014 and DOE 2016). Uranium can be found in evaporites outside the uranium plume, but at lower concentrations. Thus, uranium is released to the shallow groundwater outside the plume footprint during flooding or large recharge events, but at concentrations that are much lower than those released over the uranium plume. Release of uranium outside the uranium plume (well 0852) can exceed site standards for a period of time, depending on the interval between extreme events. Molybdenum is not found in significant concentrations in the evaporites outside of the molybdenum plume, and thus, it is a more unique indicator of mill-derived contamination.

Uranium and molybdenum are released to the shallow groundwater during evaporite dissolution with flooding or large recharge events, but may have additional geochemical controls. Extended periods of high water tables (like in the spring of 2017) appear to create reducing conditions at the top of the water table (top ports of multilevel wells that are typically dry) that can release manganese and iron. The data suggest that molybdenum that may have been sorbed to the manganese and iron is released to the groundwater. However, uranium concentrations are lower at the top of the water table, possibly due to stronger sorption to organic carbon with the greater reducing conditions. The change in geochemical conditions with extended high water table conditions is also suggested by the release of dissolved organic carbon and higher carbon dioxide concentrations that can dissolve more calcite and increase the alkalinity concentrations. These reactions are best demonstrated in well ports 857-1 and 858-1. Overall, uranium and molybdenum release from the silt layer is likely dominated by association with evaporite dissolution. However, additional mechanisms, such as sorption/desorption from iron/manganese oxides and organic carbon, along with variable redox conditions, also need to be considered in evaluating uranium and molybdenum transport.

Each multilevel well has subtle differences based on its location. Well 0852 shows evaporite dissolution with some uranium release, but does not have molybdenum (outside of the molybdenum plume). Wells 0853 and 0854 are on the edge of the uranium and molybdenum plumes. They show some potential release of uranium and molybdenum during flood or large recharge events, but trends are subtle, with molybdenum near or below the detection limit and uranium concentrations near the site standard. Wells 0855–0858 are all within the uranium and molybdenum plumes. These wells all show evaporite dissolution along with uranium and molybdenum release after flooding and large recharge events, with subtle differences. Well 0855 shows an overall more muted concentration response with the bottom port also being lower in constituent concentrations. Due to the thick silt layer at this location, the bottom port appears to have limited geochemical responses to surficial recharge events. The May 2016 flood response is seen first in the top two ports and slightly later in the bottom two ports. The high water tables at the site in April and May of 2017 are not seen in well 0855 due to its strong connection with the Little Wind River stage, but constituent increases in this time period are still evident. In well 0856, large constituent increases (except for calcium and iron) are seen after the May 2016 flood

and the high recharge in the spring of 2017. The largest 2016 response was slightly delayed and occurred in the bottom of the aquifer. The 2017 response occurred steadily in the spring throughout the aquifer. Well 0857 does not have a distinct silt layer, but has silty gravel near the surface. This well also shows a delayed response to the May 2016 flooding—albeit, this well was just near the edge of the surficial flooding. Well 0858 is the best example of evaporite dissolution after flooding or large recharge events, with a strong initial response in the top two ports and a strong response in all ports within a month. In the spring of 2017 all dissolved constituents show a continued increase from April through July, except for the dilution in port 1 during that time period for K, Mg, Na, Ca, U, SO_4, and Cl, which is likely due to the short time between flooding events, which did not allow time for evaporites to reform.

5.0 Implications

For natural flushing, long-term contaminant release—in this case, for uranium and molybdenum—can be delayed by retention in the unsaturated zone (in this case, also a silt layer with a large wicking potential). As a result, these contaminants are released only during large recharge events that force recharge water through the typically unsaturated zone.

Because of uncertainty in the timing of large recharge events, prediction of a natural flushing time frame cannot be deterministic and will need to be done in a probabilistic manner. In addition to contaminant release timing, contaminant concentrations may increase in the unsaturated zone when the time period between high recharge events becomes greater. Thus, contaminant release concentrations will also need to be considered in a probabilistic manner.

For the Riverton site, the three years of monitoring data at multilevel monitoring wells provided in this report can provide information on anticipated contaminant release concentrations. These concentrations and spikes during high recharge events will need to be compared with existing solid-phase data, expected reconcentration times, and average flood/high recharge event timing to provide a probabilistic model of natural flushing times. Such a model will be necessary to decide on future site management strategies.

6.0 References

40 CFR 192. U.S. Environmental Protection Agency, "Health and Environmental Protection Standards for Uranium and Thorium Mill Tailings," *Code of Federal Regulations*.

Ben Ahmed, S., M.M. Tlili, M. Amami, and M. Ben Aamor, 2014. "Gypsum Precipitation Kinetics and Solubility in the NaCl–$MgCl_2$–$CaSO_4$–H_2O System," *Industrial & Engineering Chemistry Research* 53(23):9554–9560, DOI:10.1021/ie5004224.

Dam, W.L., S. Campbell, R.H. Johnson B.B. Looney, M.E. Denham, C.A. Eddy-Dilek, and S.J. Babits, 2015. "Refining the Site Conceptual Model at a Former Uranium Mill Site in Riverton, Wyoming, USA," *Environmental Earth Sciences* 74(10):7255–7265, DOI:10.1007/S12665-015-4706-y.

DOE (U.S. Department of Energy), 1991. *Riverton Wyoming Final Completion Report*, Albuquerque Operations Office, Albuquerque, New Mexico, December.

DOE (U.S. Department of Energy), 1998a. *Final Site Observational Work Plan for the UMTRA Project Site at Riverton, Wyoming*, U0013801, Grand Junction Office, February.

DOE (U.S. Department of Energy), 1998b. *Final Ground Water Compliance Action Plan for the Riverton, Wyoming, Title I UMTRA Project Site*, attached to letter from DOE to NRC, Grand Junction Office, September 22.

DOE (U.S. Department of Energy), 2013. *2012 Enhanced Characterization and Monitoring Report, Riverton, Wyoming, Processing Site*, LMS/RVT/S09799, Office of Legacy Management, Grand Junction, Colorado, June.

DOE (U.S. Department of Energy), 2014. *Evaluation of Mineral Deposits Along the Little Wind River, Riverton, Wyoming, Processing Site*, LMS/RVT/S12020, Office of Legacy Management, December.

DOE (U.S. Department of Energy), 2016. *2015 Advanced Site Investigation and Monitoring Report, Riverton, Wyoming, Processing Site*, LMS/RVT/S14148, Office of Legacy Management, September.

DOE (U.S. Department of Energy), 2019. *DRAFT 2018 Verification Monitoring Report, Riverton, Wyoming, Processing Site*, LMS/RVT/S22290, Office of Legacy Management.

Drever, J.I., 1997. *The Geochemistry of Natural Water: Surface and Groundwater Environments*, 3rd Ed., Prentice-Hall, New Jersey.

Environmental Sciences Laboratory Procedures Manual, LMS/PRO/S04343, continually updated, prepared by Navarro Research and Engineering, Inc., for the U.S. Department of Energy Office of Legacy Management.

Parkhurst, D.L., and C.A.J. Appelo, 2013. "Description of Input and Examples for PHREEQC Version 3: A Computer Program for Speciation, Batch-Reaction, One-Dimensional Transport, and Inverse Geochemical Calculations," *U.S. Geological Survey Techniques and Methods*, Book 6, Chapter A43, available at https://pubs.usgs.gov/tm/06/a43/.